Catalysis Science & Technology

ROYAL SOCIETY OF CHEMISTRY

REVIEW

View Article Online
View Journal | View Issue

Cite this: *Catal. Sci. Technol.*, 2025, **15**, 2104

Recent progress and perspective of electrocatalysts for the hydrogen evolution reaction

Jianjun Shi,[ab] Yong Bao,[b] Rongrong Ye,[b] Ju Zhong,[d] Lijing Zhou,*[b] Zhen Zhao,*[bc] Wanli Kang*[a] and Saule B. Aidarova*[a]

Electrocatalytic water splitting represents a highly promising technology for the sustainable production of clean hydrogen fuel. The primary focus of research in this domain revolves around the development of efficient electrocatalysts for the hydrogen evolution reaction (HER), with the objective of minimizing the energy barrier and overall energy consumption associated with the HER process, thereby significantly reducing the overall electrical energy usage. This article initially presents a comprehensive overview of the fundamental principles underlying electrocatalytic HER, encompassing its reaction mechanism and the pertinent parameters employed for evaluating the performance of HER electrocatalysts. Following this, the article explores an in-depth exploration of the diverse range of catalysts that are commonly employed in the field of electrocatalytic HER, such as metals, oxides, sulfides, selenides, carbides, phosphides, nitrides, borides, single-atom catalysts, and carbon-supported catalysts. Particular attention is devoted to discussing the unique preparation techniques, structural characteristics, performance attributes, and the corresponding mechanistic insights pertaining to these catalysts. Lastly, this article delineates the future trajectories for the advancement of HER electrocatalysts and undertakes an analysis of the challenges that lie ahead. The primary aim of this review is to serve as a valuable reference for future research and development endeavors in the realm of HER electrocatalysts, thereby fostering the widespread adoption of water electrolysis technology.

Received 1st December 2024,
Accepted 29th January 2025

DOI: 10.1039/d4cy01449a

rsc.li/catalysis

1. Introduction

Over the past decade, the world's energy demand has undergone rapid expansion driven by the continuous growth of the population and the accelerated development of global industrialization.[1–3] Current statistics reveal that traditional fossil fuels, including coal, oil, and natural gas, still account for more than 60% of global energy consumption. In contrast, renewable energy sources such as solar, wind, tidal, and geothermal energy contribute less than 40%. This significant reliance on fossil fuels not only accelerates their depletion but also leads to a range of severe environmental issues, including air pollution and global warming. Consequently, there is an urgent necessity to develop renewable and clean energy to address these challenges and achieve sustainable long-term development. Hydrogen, as a viable new energy carrier that can replace traditional fossil fuels, is regarded as one of the most promising clean energy sources due to its high energy density and zero-emission.[4–7] Currently, the predominant method for hydrogen production is steam reforming of methane, a process characterized by low conversion efficiencies and substantial CO_2 emissions. In this context, alternative techniques such as thermal catalysis, photocatalysis, and electrocatalysis for water splitting present promising solutions. Among these technologies, electrocatalytic water splitting has gained significant attention in global research due to its ability to generate environmentally benign high-purity hydrogen. This approach utilizes electricity to facilitate hydrogen production and can be effectively integrated with intermittent energy sources like wind and solar power to enhance the overall efficiency of sustainable energy systems. Water splitting involves two half-reactions: the anode oxygen evolution reaction (OER) and the cathode hydrogen evolution reaction (HER). The efficiency and performance of HER, as the critical step in water splitting for hydrogen generation, directly impact both the energy efficiency and cost-effectiveness of the entire production

[a] *Kazakh-British Technical University, Almaty 050000, Kazakhstan. E-mail: kangwanli@upc.edu.cn, s.aidarova@kbtu.kz*
[b] *Institute of Catalysis for Energy and Environment, College of Chemistry and Chemical Engineering, Shenyang Normal University, Shenyang 110034, China. E-mail: zlj9333@163.com, zhenzhao@cup.edu.cn*
[c] *State Key Laboratory of Heavy Oil Processing, China University of Petroleum, Beijing 102249, China*
[d] *PetroChina Jianghan Machinery Research Institute Co., Ltd., Wuhan 430021, China*

process.[8–10] Given the rising global energy demand coupled with increasing environmental awareness, developing efficient and stable HER electrocatalysts has become a central focus in energy chemistry field.[11–13]

Recent advancements in nanotechnology, materials science, and computational chemistry have significantly accelerated research on the HER. Specifically, researchers have improved both the activity and stability of electrocatalysts by designing and synthesizing nanomaterials with distinct morphologies and compositions.[14] For instance, the incorporation of innovative porous materials such as MOFs and COFs as templates or precursors facilitates the development of electrode materials characterized by high specific surface areas and abundant active sites. Concurrently, progress in computational chemistry has substantially advanced investigations into HER mechanisms. Utilizing techniques such as quantum chemical calculations and molecular dynamics simulations enables researchers to achieve a comprehensive understanding of the underlying mechanisms and kinetic processes associated with HER. This elucidates the intrinsic relationship between electrocatalyst activity and its structural attributes, thereby providing a solid theoretical foundation for the rational design and optimization of electrocatalyst for HER.[15–17]

Researchers have made significant strides in the discovery of novel non-precious metal catalysts. Compared to traditional precious metal catalyst, non-precious metal catalysts offer advantages such as lower costs and abundant availability, thereby demonstrating greater potential for practical applications.[18–20] Currently, a variety of non-noble metal catalysts, including transition metal sulfides, phosphides, and nitrides, have exhibited commendable efficacy in HER.[21–23] Despite significant advancements in the research on HER, several challenges remain persistent. These challenges encompass the enhancement of both catalyst activity and stability, as well as the resolution of issues pertaining to large-scale preparation and industrial application of these catalysts. Consequently, future research should prioritize a deeper understanding of the HER mechanism and kinetic processes, alongside the development of new efficient and stable catalysts for practical implementation in water electrolysis.[24–26] The advancements in HER, as a fundamental step in water splitting, hold profound implications for fostering innovation in renewable energy and environmental protection technologies.[27–29] Given the continuous emergence of novel materials, technologies, and methodologies, there is compelling anticipation that future investigations into HER will yield substantial outcomes that significantly contribute to sustainable development efforts globally.[30–32] In light of escalating global energy demands coupled with intensifying concerns regarding environmental pollution, pursuing renewable clean energy conversion and storage technologies has emerged as a pivotal area of scientific inquiry. Water electrolysis for hydrogen production has garnered considerable attention from both academic researchers and industry stakeholders alike due to its efficiency and eco-friendliness.[33–35] The performance of HER directly influences both the efficiency and cost-effectiveness of the entire hydrogen production process.[36–38] Therefore, comprehensive examination of HER mechanisms along with optimization strategies for catalysts and electrode materials are crucial to advancing electrolysis technology.

2. The mechanism of HER

HER refers to the process by which water molecules are reduced on the cathode surface during water electrolysis to produce hydrogen. This multi-step reaction involves electron transfer, ion migration, and surface chemical reactions, with its performance being influenced by various factors, including catalysts, and electrolytes. Consequently, a comprehensive understanding of the HER mechanism is essential for guiding the design and optimization of catalysts. The HER process consists of three distinct steps: the electrochemical hydrogen adsorption reaction (Volmer reaction), the electrochemical desorption reaction (Heyrovsky reaction) and the chemical desorption reaction (Tafel reaction). The HER process can be described using the following elementary steps.[39]

Acidic medium:

$$H^+ + e^- \rightarrow H^* \text{ (Volmer)}$$

$$H^* + H^+ + e \rightarrow H_2 \text{ (Heyrovsky)}$$

$$H^* + H^* \rightarrow H_2 \text{ (Tafel)}$$

Alkaline medium:

$$H_2O + e^- \rightarrow H^* + OH^- \text{ (Volmer)}$$

$$H^* + H_2O + e^- \rightarrow OH^- + H_2 \text{ (Heyrovsky)}$$

$$H^* + H^* \rightarrow H_2 \text{ (Tafel)}$$

where * represents an active site on the electrode surface, and H* is the hydrogen atom adsorbed on the active site.

The HER initiates with an electrochemical hydrogen adsorption step. In this step, either adsorbed hydrogen ions (in acidic media) or water molecules (in basic media) on the surface of the hydrogen evolution electrode are coupled with electrons to generate a hydrogen atom intermediate (H*) at the active site. Subsequently, competitive or synergistic electrochemical desorption and chemical desorption reactions take place on the electrode surface. The electrochemical desorption primarily involves the combination of H* and electrons with H^+ (under acidic

conditions) or water molecule (under basic conditions) to form H_2. Conversely, the chemical desorption reaction occurs through the coupling of two H* to produce H_2, regardless of whether in acidic or basic media.

In acidic solutions, protons first attach to the surface of the electrocatalyst through diffusion and are subsequently reduced to molecular H_2. On one hand, if the hydrogen binding energy (HBE) is too weak, it will lead to a low concentration of protons adsorbed on the surface of the solid electrocatalyst. On the other hand, if the HBE is too strong, it will cause the active sites of the catalyst to be persistently occupied by adsorbed H, leading to catalyst poisoning. The Gibbs free energy of hydrogen adsorption (ΔG_{H^*}) serves as a crucial indicator for assessing the change in Gibbs free energy during the HER process and can be used to evaluate the adsorption of active H and the desorption of H_2. Under ideal conditions, ΔG_{H^*} should approach zero, at which point the corresponding exchange current density (j_0) reaches its maximum value, and the HER activity also attains its highest level. In alkaline or neutral solutions, due to the almost non-existent free H^+, H* primarily originates from the dissociation process of water ($H_2O + * \leftrightarrow H^* + OH^-$). Furthermore, the Heyrovsky reaction process ($H^* + H_2O + e^- \rightarrow H_2 + OH^-$) also involves the dissociation step of water molecules. Therefore, in the HER process under alkaline conditions, the slow kinetic characteristics are primarily attributed to the high energy barrier that must be overcome for the additional water dissociation step.

Throughout the HER process, electrical energy is efficiently converted into chemical energy, which is subsequently stored in the produced hydrogen gas. The efficiency of HER is intrinsically linked to the adsorption and desorption processes occurring at the electrode surface. During this reaction, either water molecules or hydrogen ions must first adsorb onto the electrode surface, followed by interactions with the active sites present on the surface of electrode. This interaction facilitates hydrogen gas generation through electron transfer and surface chemical reactions, after which hydrogen gas desorbs from the electrode surface. Therefore, optimizing both adsorption and desorption processes at the electrode interface, as well as increasing both the quantity and intrinsic activity of active sites, is essential for enhancing HER performance.[40,41]

3. Catalysts for HER

The role of catalysts in HER is to promote the transfer of electrons and the conversion of water molecules. These catalysts usually have specific active sites that can effectively adsorb water molecules and significantly lower the activation energy required for the reaction, allowing HER to occur at lower potentials. In recent years, significant progress has been achieved in designing novel catalysts and optimizing their structures and performance.

3.1 Metal

Noble metal catalysts such as platinum (Pt), palladium (Pd), and iridium (Ir) are considered the ideal catalyst choice for the HER due to their excellent conductivity, stability, and strong adsorption of hydrogen.[42–45] Precious metal catalysts provide active sites that can effectively adsorb water molecules and promote electron transfer, thereby accelerating HER. Specifically, these precious metal catalysts can adsorb water molecules in the electrolyte on their surfaces and catalyze the reduction reaction of water molecules to generate hydrogen and hydroxide ions. Meanwhile, the excellent conductivity of precious metal catalysts can ensure that electrons are quickly transmitted across the catalyst surface, further enhancing the reaction rate.

While noble metal catalysts exhibit superior performance in the HER, their prohibitive cost limits their widespread application. Consequently, contemporary research efforts are predominantly focused on minimizing the quantity of noble metals used and enhancing their catalytic activity. On the one hand, researchers optimize the preparation method of the catalyst by using nanotechnology to prepare noble metal catalysts with specific morphology and size to increase their specific surface area and active site number.[46–48] On the other hand, researchers introduce other metals or non-metallic elements to form alloys or composites with noble metals to regulate the electronic structure and surface properties of the catalyst, thereby further improving its catalytic activity.[49–52]

Duan *et al.*[53] systematically investigated the hydrogen adsorption behavior on platinum nanowires (PtNWs) by integrating electrical transport spectroscopy (ETS) with ReaxFF reactive force field calculations. The ETS results clearly revealed the presence of two distinct hydrogen adsorption peaks on PtNWs. Specifically, one peak was observed at 0.20 V relative to the reversible hydrogen electrode (RHE), which is associated with hydrogen adsorption on the (111) and (100) facets. The other peak, appearing at 0.038 V RHE, was attributed to hydrogen adsorption on edge sites. Both experimental and computational results consistently demonstrated that hydrogen adsorption on edge sites (HOPD) aligns closely with the onset potential of HER. Moreover, the activation energy for HER at edge sites was found to be significantly lower than that at facet sites, thus underscoring the predominant role of edge sites in the HER process. Furthermore, the study revealed that hydrogen adsorption on edge sites is markedly suppressed in alkaline media, resulting in a substantial decrease in HER kinetics. These findings not only elucidate the long-standing ambiguities regarding the roles of different sites on the platinum surface but also offer invaluable insights for the design of HER catalysts. Cheng *et al.*[54] successfully synthesized PdPt alloys with varying thicknesses of Pt shells using a wet chemical method, specifically including $PdPt_{2L}$ with a double-layer Pt shell and $PdPt_{ML}$ with

multi-layer Pt shells. In a 0.5 M H_2SO_4, $PdPt_2L$ requires only an overpotential of 18 mV to achieve a current density of 10 mA cm^{-2}, and its HER process follows the Volmer–Tafel mechanism with rapid kinetics for hydrogen generation, as shown in Fig. 1a–c. Furthermore, $PdPt_2L$ can operate stably for at least 510 hours at a current density of 110 mA cm^{-2} without significant decay in catalytic activity. Remarkably, in a proton exchange membrane water electrolyzer, the $PdPt_2L||IrO_2$ system maintains stable operation for 100 hours at a high current density of 500 mA cm^{-2}, with a voltage degradation rate of only 1.69 mV h^{-1}. *In situ* Raman spectroscopy results indicate that Pt sites serve as active species that preferentially capture hydrogen atoms, which facilitates the HER process. Operando electrochemical impedance spectroscopy (EIS) analysis further reveals that the reaction resistance of $PdPt_2L$ is primarily determined by the interfacial charge transfer resistance, rather than the electron transfer resistance at the catalytic inner layer/interface. Additionally, density functional theory (DFT) calculations show that the weak strain effect of $PdPt_2L$ effectively reduces the hydrogen adsorption energy, which favors the desorption of H* and the generation of H_2, thereby accelerating the kinetics of the HER process (Fig. 1d).

Song *et al.*[55] successfully synthesized a nickel nitride (Ni_3N)-supported catalyst featuring a highly exposed Pt(110) crystal facet, denoted as Pt(110)–Ni_3N, on a vacancy-rich $Ni(OH)_2$ substrate through a two-step process involving impregnation and calcination. X-ray photoelectron spectroscopy (XPS) and X-ray absorption near-edge structure (XANES) analyses revealed that there is a strong interaction between Pt and Ni_3N, which promotes electron transfer from Pt to Ni atoms within Ni_3N, consequently decreasing the electron density on the Pt surface. DFT studies further elucidated that this alteration in electron density on the Pt surface significantly affects the adsorption geometry and energy of H* on the Pt(110) crystal facet, as illustrated in Fig. 2a and b. As a result, the Pt(110)–Ni_3N catalyst exhibits outstanding HER performance in 0.5 M H_2SO_4. Dai *et al.*[56] adeptly integrated the advantages of Pd–M and PdH_x structures, successfully synthesizing a palladium–copper

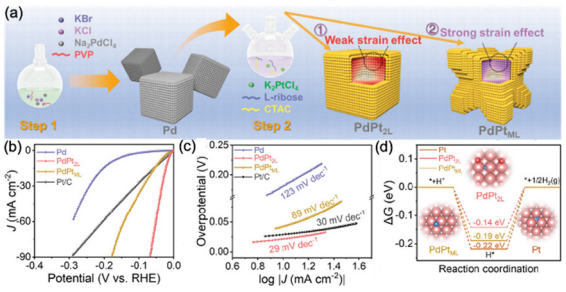

Fig. 1 (a) The synthesis schematic illustration of $PdPt_{2L}$ and $PdPt_{ML}$. (b) LSV polarization curves between Pd, $PdPt_{2L}$, $PdPt_{ML}$, and commercial Pt/C. (c) Tafel slopes. (d) ΔG_{H^*} on Pt sites of $PdPt_{2L}$ and $PdPt_{ML}$, and Pt. The insets are atomic structure simulation model of $PdPt_{2L}$, $PdPt_{ML}$, and Pt with adsorbed hydrogen.[54]

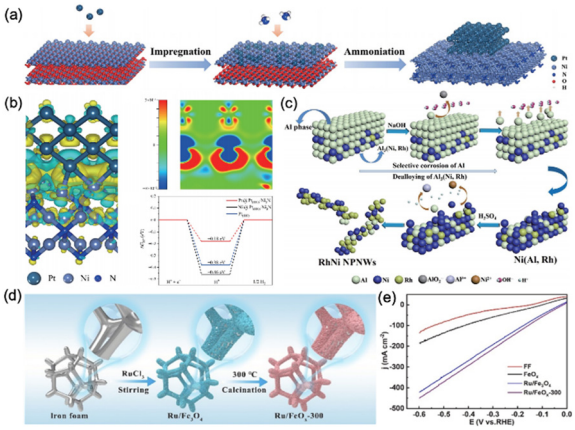

Fig. 2 (a) The synthesis schematic illustration of Pt(110)–Ni_3N. (b) The DFT calculations of Pt(110)–Ni_3N.[55] (c) Schematic illustration showing the dealloying mechanism of the $Al_{97.8}Ni_2Rh_{0.2}$-0 precursor.[57] (d) Schematic illustration for the synthesis of Ru/FeO_x-300. (e) HER polarization curves of different catalysts.[58]

hydride catalyst ($PdCu_{0.2}H_{0.43}$). During the synthesis process, the metal precursors first underwent co-reduction in an oleylamine system to form a Pd–Cu alloy. Subsequently, this alloy was uniformly mixed with carbon black in a hexane solvent. Finally, the mixture was subjected to calcination under ambient conditions, a process that enabled the successful intercalation of hydrogen atoms into the lattice interstitials of the Pd–Cu alloy. Utilizing advanced techniques such as aberration-corrected transmission electron microscopy (AC-TEM), X-ray diffraction (XRD), and X-ray absorption spectroscopy (XAS), the morphology and structure of the catalyst were thoroughly characterized, confirming the alloy hydride structural features of the resultant Pd–Cu–H catalyst. Furthermore, the $PdCu_{0.2}H_{0.43}$ catalyst effectively suppressed the oxidation of Pd, maintaining its metallic state. This method not only achieved the interstitial insertion of hydrogen atoms at atmospheric pressure but also endowed the catalyst with exceptional performance and stability for HER. DFT calculations revealed that the synergistic effects of hydride formation and copper alloying in the $PdCu_{0.2}H_{0.43}$ catalyst not only optimized hydrogen adsorption capabilities but also enhanced the structural stability of the catalyst, thereby enabling long-term stable HER performance. Zhang *et al.*[57] proposed a novel synthesis method by integrating a self-templating strategy involving eutectic solidification, microalloying, and chemical dealloying process, successfully preparing one-dimensional nanoporous RhNi alloy nanowires, as shown in Fig. 2c. By precisely tuning the solidification conditions, the length of the RhNi nanowires can be effectively controlled. The as-prepared RhNi catalyst exhibits excellent electrocatalytic activity and stability for HER in both acidic and alkaline media. DFT calculations reveal that the ΔG_{H^*} on the $Rh_3Ni_2(111)$ surface is comparable to that on the Pt(111) surface, indicating that the bonding strength between the intermediate and the active site is optimized, thereby endowing Rh_3Ni_2 with HER

catalytic activity comparable to Pt. Furthermore, when H adsorbs on the metal surface, significant orbital interaction occurs between the s orbital of H and the d orbital of Rh, forming a stable Rh–H bond.

Significant advancements have been achieved in the development of novel precious metal catalysts. For instance, researchers have identified specific composite catalysts comprising precious metals and iron foam or carbon materials that exhibit superior performance in HER. Zhao *et al.*[58] reported a spherical Ru/FeOx composite supported on foam iron for overall water splitting in neutral media through a synchronous heating and stirring treatment followed by calcination process. Specifically, the Ru/FeO_x-300 sample demonstrated remarkable HER activity, with an overpotential of only 30 mV at a current density of 10 mA cm^{-2}, and a Tafel slope of 7.3 mV dec^{-1} in 1.0 M phosphate buffer solution, as illustrated in Fig. 2d and e. The synergistic effect between Ru and FeO_x, coupled with the unique spherical structure of the composite, not only effectively enhanced the overall conductivity of the catalyst but also promoted the exposure of a large number of active sites, thereby augmenting its electrocatalytic performance. XPS analysis of the catalyst after the catalytic reaction revealed a positive shift in the Fe 2p peak and a negative shift in the Ru 3p peak, indicating electron transfer from Fe to Ru. This electron transfer mechanism significantly enhanced the catalytic activity of Ru atoms. These catalysts not only reduce the amount of precious metal required but also substantially enhance both stability and catalytic activity, thereby paving a new avenue for the optimized design of HER catalysts.[59]

Transition metal catalysts, such as iron (Fe), cobalt (Co), and nickel (Ni), have exhibited significant catalytic activity in the electrocatalytic HER owing to their exceptional conductivity and chemical stability. The abundant d electrons of these transition metals provide active sites conducive to efficient hydrogen production. Moreover, the catalytic performance of these metals can be optimized through modifications to their electronic structure, lattice configuration, and surface characteristics. The diversity among transition metal elements also presents a broad spectrum of options for the design and development of effective HER catalysts.

Jiang *et al.*[47] successfully designed and synthesized a high-entropy NiFeCoCuTi alloy on the surface of columnar nanoporous nickel scaffolds. The catalyst exhibited excellent HER performance in 1 M KOH, achieving an ultrahigh current density of 2 A cm^{-2} with an overpotential of only 209 mV, and maintaining outstanding stability for over 240 hours. Through XPS characterization, it was found that significant electron transfer occurred from Ti atoms to Ni, Co, and Fe atoms in the high-entropy alloy NiFeCoCuTi, and the surface Ti atoms were predominantly in the oxidized state. This oxidized state of Ti atoms facilitated the adsorption of OH, thereby promoting the formation of optimal ΔG_{H^*} multi-site electrocatalytic centers associated with the NiFeCoCu surface alloy. In conjunction with the results of electrocatalytic performance tests, it can be clearly concluded that the presence of Ti atoms plays a crucial role in enhancing the activity of the electrocatalytic HER. Peng *et al.*[60] prepared a series of Ni–Mo alloys with varying molybdenum contents *via* an electrodeposition method, and subsequently obtained alloy catalysts with a preferentially exposed $MoNi_4$(312) crystal plane through electrochemical reconstruction. In acidic electrolyte, the reconstructed catalyst exhibited an overpotential of 23 mV at a current density of 10 mA cm^{-2}, accompanied by a Tafel slope of 53.9 mV dec^{-1}, outperforming commercial Pt/C catalysts. Furthermore, the catalyst also demonstrated satisfactory HER performance in alkaline electrolyte. DFT calculations revealed that the strong interaction between Ni and Mo atoms on the $MoNi_4$(312) crystal plane facilitated electron transfer from Ni to Mo, optimizing the electronic structure and reducing the hydrogen adsorption energy, thereby accelerating the HER process. Additionally, the $MoNi_4$(312) crystal plane possessed high corrosion resistance, contributing to the long-term stability of the catalyst.

Soo-Kil Kim *et al.*[61] successfully prepared Cu_xMo_{100-x} (where x represents the atomic percentage of Cu) catalysts on titanium (Ti) substrates *via* electrodeposition. By precisely adjusting the composition of the electrolyte, they effectively controlled the atomic concentrations of Cu and Mo, thereby achieving fine-tuning of the catalyst's composition and structure. XPS analysis provided deep insights into the electronic interaction mechanism between Cu and Mo elements, revealing that the incorporation of Mo rendered Cu in an electron-rich state. This characteristic significantly facilitated the hydrogen adsorption and desorption processes. Subsequently, the research team deposited the $Cu_{93.7}Mo_{6.3}$ catalyst onto carbon paper and employed it as the cathode, while IrO_2 was used as the anode, to successfully assemble a proton exchange membrane water electrolyzer single cell. Performance tests were conducted on the single cell under operating conditions at 90 °C. The test results demonstrated that a current density of 0.50 A cm^{-2} was achieved at a cell voltage of 1.9 V. Although this current density was slightly lower than that of cells employing Pt cathodes, the activity based on metal mass (3.4 A mg^{-1} metal) was significantly higher than that reported for previous PEMWE systems, fully showcasing the excellent performance of the prepared catalyst.

Transition metal compounds, including metal sulfides, phosphides, nitrides, carbides, and selenides, serve as effective catalysts in the electrocatalytic HER. To optimize the performance of these transition metal compound catalysts, various strategies have been employed. One approach involves precise control over the nanostructure of the catalyst by synthesizing nanoparticles or nanowires with specific morphologies and dimensions. This strategy effectively increases the catalyst's specific surface area, thereby exposing more active sites and significantly enhancing its catalytic activity. Another strategy entails alloying or doping with other metallic or non-metallic elements to modify the electronic

structure and surface properties of the catalyst, thus optimizing its adsorption and activation efficiency for hydrogen atoms. Additionally, modifying the catalyst surface is regarded as an effective method to improve performance. For instance, introducing appropriate functional groups or incorporating co-catalysts can enhance the surface characteristics of the catalyst and improve its ability to adsorb and activate water molecules.

The catalytic HER performances of various metal-based electrodes are compared in Table 1.

3.2 Metal oxide

Metal oxides possess the ability to reduce the activation energy of HER, thereby accelerating the process of water dissociation and hydrogen generation. Their distinctive electronic structure and chemical properties endow them with exceptional catalytic performance in electrocatalytic HER.

Zhu *et al.*[62] successfully synthesized Rh-doped hollow CoFe layered double hydroxides (LDH) utilizing ZIF-67 nanotriangles grown on foam nickel as templates. Comprehensive theoretical calculations demonstrated that the incorporation of Rh atoms conferred multiple advantages, significantly enhancing the electrocatalytic performance for both HER and OER. The introduction of Rh atoms, supported by density of states (DOS) analysis and free energy assessments, markedly improved the conductivity of CoFe LDH while simultaneously lowering the energy barrier. Moreover, Fe vacancies induced by Rh doping, along with the highly porous hollow nanostructure, optimized the HER and OER processes. Consequently, the prepared catalyst exhibited an HER overpotential of merely 28 mV at a current density of 10 mA cm^{-2}, and an OER overpotential of 245 mV at 100 mA cm^{-2}. Furthermore, when this electrocatalyst was employed for overall water splitting applications, it achieved a current density of 10 mA cm^{-2} with an impressive cell voltage of only 1.46 V. Gao *et al.*[63] successfully synthesized a composition- and morphology-tunable Co-doped $NiO/NiFe_2O_4$ mixed oxide mesoporous nanosheet array on a nickel foam substrate using a solvothermal–calcination two-step method. The densely interconnected mesoporous nanosheet array of the catalyst not only provides abundant catalytic active sites but also effectively mitigates the significant volume changes that occur during electrochemical processes. Characterization results indicate that due to the similar radii of Co and Ni atoms, the substitution of Ni atoms by Co atoms in the NiO lattice does not cause a significant change in the lattice constant. However, this substitution process leads to electron transfer from Ni atoms to Co and Fe atoms, making the electron-rich Co atoms more easily accessible to electrons and facilitating the reaction with adsorbed water molecules to generate hydrogen atoms, thereby enhancing the activity of HER. Yang *et al.*[64] employed a two-step strategy combining hydrothermal and impregnation methods to successfully synthesize uniformly distributed porous $CuMoO_4@Co_3O_4$ nanosheet electrocatalysts on a nickel foam substrate. XPS analysis revealed a significant positive shift in the binding energy of Mo^{6+} ions, indicating strong electronic interactions between $CuMoO_4$ and Co_3O_4. Furthermore, in the $CuMoO_4@Co_3O_4$ electrode system, Mo^{6+} ions can successfully oxidize Cu^+ to Cu^{2+} during HER process, a mechanism that enhances the HER performance of the $CuMoO_4@Co_3O_4$ electrode. Under 1 M KOH electrolyte conditions, the electrode exhibits an HER overpotential of 54 mV at a current density of 10 mA cm^{-2} and an OER overpotential of 251 mV at 50 mA cm^{-2}. Additionally, at a higher current density of 100 mA cm^{-2}, the HER and OER performances of the electrode demonstrate excellent stability over a continuous 120-hour test.

N. Ponpandian *et al.*[65] developed a novel three-dimensional binary nanocomposite electrode (denoted as $CC@WO_3/GR$), which comprises hexagonally oriented WO_3 nanorods and reduced graphene layers arranged on a conductive carbon nanofiber substrate (Fig. 3a). The $CC@WO_3/GR$ electrode achieved a low overpotential of merely 64 and 78 mV to reach a current density of 10 mA cm^{-2} in 0.5 M H_2SO_4 and 1 M KOH, respectively (Fig. 3b and c). The intrinsic activity of the multifunctional active sites within the $CC@WO_3/GR$ electrode plays a pivotal role in the hydrogen spillover effect (HSPE). Specifically, in acidic media, the adsorption of protons on O sites synergizes with W elements as intermediates for hydrogen spillover to the carbon supports, thereby effectively facilitating efficient H_2 gas release.

Wang *et al.*[66] successfully designed and synthesized a $Ni_{17}W_3/MoO_{3-x}/WO_{3-x}$ multicomponent catalyst using $Ni_4W_6O_{21}$ polyhedra as templates. In this catalyst, $Ni_{17}W_3$ serves as

Table 1 A comparison of catalytic HER performances for the metal-based catalysts

Catalyst	Electrolysis test	Electrolyte	Current density (mA cm^{-2})	Overpotential (mV)	Tafel slope (mV dec^{-1})	Ref.
$PdPt_{2L}$	HER	0.5 M H_2SO_4	10	18	29	54
$Pt(110)–Ni_3N$	HER	0.5 M H_2SO_4	10	33	44.9	55
$PdCu_{0.2}H_{0.43}$	HER	0.5 M H_2SO_4	10	28	23	56
$Al–Ni–Rh_2$	HER	1 M KOH	10	43.1	41.1	57
Ru/FeO_x	HER	1 M PBS	10	30	7.3	58
	OER	1 M PBS	10	212	71	
NiFeCoCuTi	HER	1 M PBS	100	159	50	47
		1 M KOH	2000	209	43	
$MoNi_4(312)$	HER	0.5 M H_2SO_4	10	23	53.9	60
		1 M KOH	10	43	92.4	

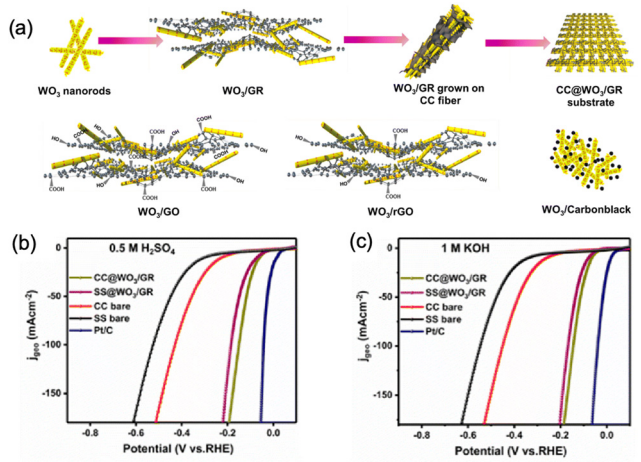

Fig. 3 (a) Schematic illustration for the synthesis of CC@WO_3/GR. Polarization curves (b) in 0.5 M H_2SO_4 and (c) in 1 M KOH.[65]

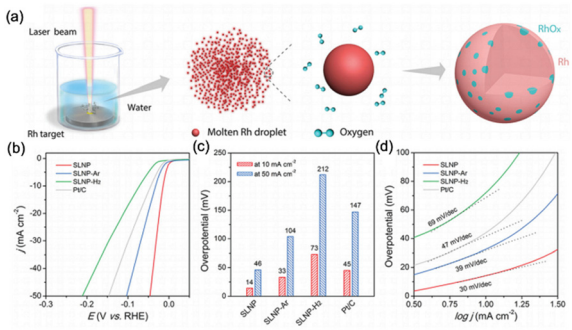

Fig. 4 (a) Schematic illustration for the synthesis of the SLNP catalyst. (b) The HER polarization curves of different catalysts. (c) Overpotentials of different catalysts derived from HER polarization curves at 10 and 50 mA cm^{-2}, respectively. (d) Tafel plots derived from the polarization curves shown in (b).[68]

the active metal phase, while MoO_{3-x}/WO_{3-x} acts as the support. By adjusting the molar ratio of MoO_3 to WO_3, the concentration of oxygen vacancies in the metal oxide support can be effectively tuned. The abundant oxygen vacancies in the MoO_{3-x}/WO_{3-x} support not only significantly enhance the hydrogen insertion/extraction kinetic performance of the metal oxide, but also improve its hydration capability. This characteristic enables efficient hydrogen adsorption/transfer/desorption kinetics on the surface and interfaces of the $Ni_{17}W_3/MoO_{3-x}/WO_{3-x}$ catalyst, thereby markedly improving its HER performance across the full pH range. DFT calculations and *in situ* Raman spectroscopy analysis reveal the mechanism of hydrogen spillover occurring at the metal/metal oxide interface, which accelerates the kinetics of hydrogen adsorption, transfer, and desorption. Cho *et al.*[67] successfully fabricated mixed-phase (Co,Ce) oxide films with varying Co/Ce molar ratios on a nickel foam substrate using an electrodeposition method. The heterogeneous interface between cobalt oxide and cerium oxide effectively facilitated rapid electron transfer, significantly reducing the adsorption energy of reaction intermediates, and thereby greatly accelerating the reaction kinetics. The optimized material, $Co_{0.85}Ce_{0.15}$, exhibited a low overpotential of 76 mV for HER at a current density of 10 mA cm^{-2}. Du *et al.*[68] successfully designed and synthesized a strawberry-like nanostructure with RhO_2 clusters embedded in the surface layer of Rh nanoparticles (SLNP) using a laser ablation method in aqueous rhodium, as shown in Fig. 4a. Due to the lattice mismatch between the RhO_2 clusters and the Rh substrate, a significant compressive strain effect was induced. This compressive strain not only effectively stabilized the RhO_2 clusters but also significantly enhanced their HER catalytic performance. In 1 M KOH solution, when the current density reached 10 mA cm^{-2}, the overpotential was only 14 mV, and the Tafel slope was reduced to 30 mV dec^{-1} (Fig. 4b–d). Further DFT calculations revealed that the compressive strain promoted electron transfer from Rh to O, enhancing the stability of the Rh–O bonds. Moreover, this strain facilitated the electron transfer process from adsorbed water molecules to RhO_2, resulting in a decrease in the number of electrons in the water molecules and a weakening of the hydrogen–oxygen bond strength, thereby promoting the dissociation reaction of water.

The catalytic HER performances of various metal electrodes are compared in Table 2.

3.3 Metal sulfide

Sulfide catalysts, primarily composed of transition metal sulfides (TMSs) such as molybdenum disulfide (MoS_2) and tungsten disulfide (WS_2), are widely employed to enhance the efficiency of hydrogen production through water electrolysis. These sulfides exhibit distinct physicochemical properties, including tunable electronic structures, an abundance of surface-active sites, excellent electrical conductivity, and chemical stability, which render them highly suitable for HER. Sulfide catalysts demonstrate superior electrocatalytic performance in water electrolysis by effectively facilitating hydrogen activation and reducing the energy barrier associated with proton reduction. Furthermore, these sulfide-based HER catalysts exhibit exceptional stability and durability, maintaining their catalytic activity over extended periods of electrolysis. To further optimize the performance of these catalysts, researchers have adopted various strategies, including the optimization of catalyst morphology, size, and structure, modulation of active sites, and compounding with other materials. These strategies can significantly enhance the catalytic activity and stability of the catalysts, thereby promoting the development and application of hydrogen production technologies derived from water electrolysis.

Table 2 A comparison of catalytic HER performances for the metal oxide-based catalysts

Catalyst	Electrolysis test	Electrolyte	Current density (mA cm^{-2})	Overpotential (mV)	Tafel slope (mV dec^{-1})	Ref.
Rh-doped CoFe-ZLDH@NF	HER	1 M KOH	10	28	42.8	62
	OER	1 M KOH	100	245	—	
Co-doped NiO/$NiFe_2O_4$	HER	1 M KOH	10	84	53.6	63
	OER	1 M KOH	10	186	38.5	
$CuMoO_4$@Co_3O_4	HER	1 M KOH	10	54	98.8	64
	OER	1 M KOH	50	251	87.4	
CC@WO_3/GR	HER	0.5 M H_2SO_4	10	84	66	65
		1 M KOH	10	93	72	
$Ni_{17}W_3/MoO_{3-x}/WO_{3-x}$	HER	0.5 M H_2SO_4	10	14	32.6	66
		1 M PBS	10	42	73.9	
		1 M KOH	10	16	34.9	
$Co_{0.85}Ce_{0.15}$	HER	1 M KOH	10	76	92.4	67
	OER	1 M KOH	20	177	85.02	
RhO_2	HER	1 M KOH	10	14	30	68

Ren *et al.*[69] have for the first time employed electrochemical tip-enhanced Raman spectroscopy (EC-TERS) to dynamically characterize the lattice structure and electronic properties of active sites in molybdenum disulfide (MoS_2) during the electrocatalytic HER (Fig. 5a). Their study reveals that the edge sites of MoS_2 serve as the active sites for HER, undergoing significant structural reconstruction during the reaction process, which encompasses the rearrangement of the lattice structure and changes in electron density. Furthermore, the electrochemical activation process further enhances the catalytic activity of the edge sites, potentially through the loss of sulfur atoms, leading to structural strain. Li *et al.*[70] employed Cu nanodots-decorated Ni_3S_2 nanotubes deposited on carbon fibers (Cu NDs/Ni_3S_2 NTs-CFs) as a catalyst, achieving efficient HER performance in an alkaline environment. The analysis results of Raman spectroscopy and XPS indicated that strong electronic interactions occurred between Cu and Ni_3S_2, leading to a decrease in electron density on Cu and a corresponding increase on Ni_3S_2. During the HER process, positively charged Cu effectively adsorbed and activated water molecules by capturing the O atoms, thereby promoting the cleavage of H–O bonds. Meanwhile, negatively charged Ni_3S_2 weakened the S–H_{ads} bonds, optimizing the adsorption and desorption process of H*. DFT calculations further confirmed that the Cu/Ni_3S_2 composite exhibited optimal adsorption of H, leading to high HER electrocatalytic activity, as shown in Fig. 5b–d. Su *et al.*[71] successfully synthesized high-performance MoS_2 electrocatalysts with surface sulfur vacancies *via* a facile hydrothermal method, using hydrochloric acid as a sulfur etchant. Compared to pristine MoS_2, the MoS_2 electrocatalysts engineered with surface sulfur vacancies exhibited significantly enhanced HER performance, with a performance improvement of up to 32-fold. Impedance analysis further revealed that when the concentration of surface sulfur vacancies was at a low level, it effectively optimized the charge transfer process; whereas at higher concentrations, it significantly promoted the desorption process of H atoms. Additionally, the introduction of sulfur vacancies also led to a reduction in the grain size of MoS_2, which may also be a favorable factor contributing to its improved HER performance. Most importantly, this mild synthesis method is not only simple to operate but also highly versatile, with potential for extension to the preparation of other metal sulfide compounds beyond molybdenum disulfide. Chai *et al.*[72] synthesized a series of (Zn–)Co_9S_8@CF three-dimensional self-supporting materials with diverse nanostructures on copper foam substrates by precisely controlling the Zn^{2+} to Co^{2+} ratio. Compared to pure Co_9S_8 and other samples with varying ratios, the Zn–Co_9S_8@CF(1-1) material characterized by a zinc–cobalt ratio of

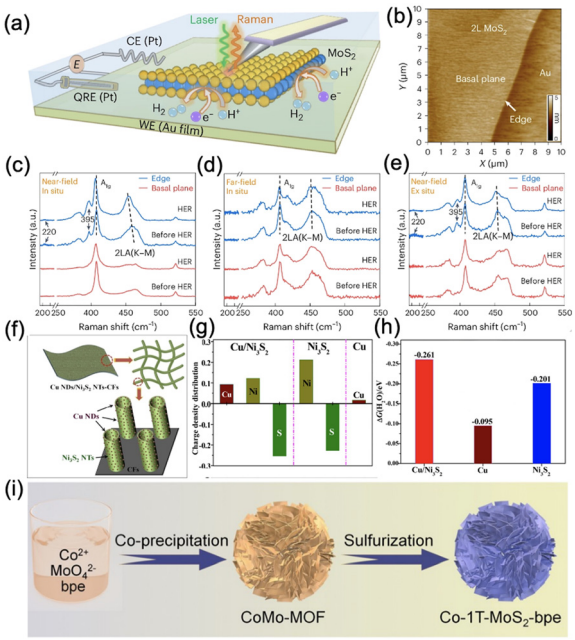

Fig. 5 (a) Schematic of the experimental set-up of EC-TERS study. (b) AFM image of the mechanically exfoliated bilayer MoS_2 on an atomically smooth gold film. (c and d) EC-situ TERS spectra, (e) *ex situ* TERS spectra of edges and basal planes.[69] (f) Schematic illustration of the microstructure of Cu NDs/Ni_3S_2 NTs-CFs. (g) The charge density distributions on Cu/Ni_3S_2, Ni_3S_2, and Cu. (h) The calculated adsorption free energy changes of H_2O on Cu/Ni_3S_2, Ni_3S_2 and Cu.[70] (i) Schematic illustration of the synthesis procedure of Co-1T-MoS_2-bpe.[73]

1 : 1 exhibits catalytic activity for HER, and long-term durability across a wide pH range. This remarkable performance can be attributed to its distinctive network structure. The three-dimensional copper foam substrate not only provides excellent conductivity but also significantly enhances the exposure of numerous active sites, thereby ensuring the material's long-term stability. Dong *et al.*[73] employed a CoMo-MOF precursor and a high-temperature sulfidation method to successfully dope Co atoms *in situ* within the basal plane of 1T-MoS_2 and insert organic bpe molecules *in situ* into the interlayer of 1T-MoS_2, thereby preparing a Co-1T-MoS_2-bpe catalyst with enlarged interlayer spacing and a nanoflower structure composed of nanosheets, as shown in Fig. 5e. The multitooth ligand 1,2-bis (4-pyridyl) ethane (bpe) can form stable connections with the two-dimensional 1T-MoS_2 layers through cobalt sites, effectively enlarging the interlayer spacing of MoS_2. This structural change not only promotes the exposure of active sites but also accelerates the water dissociation process and optimizes the adsorption and desorption behavior of H during the alkaline HER. DFT calculation results indicate that the optimization of the electronic structure of 1T-MoS_2 stems from the formation of a three-dimensional metal–organic structure by connecting π-conjugated ligands, which weakens the hybridization between the Mo 3d and S 2p orbitals, making the S 2p orbitals more prone to hybridize with the H 1s orbitals.

Yasufumi Takahashi *et al.*[74] employed high-resolution Scanning Electrochemical Cell Microscopy (SECCM) technique to conduct detailed imaging and quantitative analysis of the catalytic active sites for HER in 1H-MoS_2 nanosheets, MoS_2 and WS_2 heterostructured nanosheets. By comparing the HER activity at the edge regions, basal planes, and heterojunctions of 1H-MoS_2 nanosheets, the study revealed that the sites at the edge regions exhibited significant current response, lower overpotential, and smaller Tafel slope. Furthermore, the research also uncovered that there was no significant correlation between the HER activity and the number of layers in MoS_2 nanosheets. Zhou *et al.*[75] successfully synthesized 2H-MoS_2 materials with varying sulfur-to-molybdenum ratios (S/Mo ratios) by precisely controlling the proportions of sulfur (S) and molybdenum (Mo) precursors, enabling fine-tuned manipulation of the local atomic environment around vacancies in MoS_2 through adjustment of the Mo–S ratio (Fig. 6a). Systematic performance evaluations revealed that MoS_2 with a higher proportion of molybdenum-terminated vacancies exhibited superior HER performance compared to MoS_2 featuring sulfur-terminated vacancies and defect-free MoS_2 (Fig. 6b and c). Furthermore, advanced characterization techniques confirmed that in M-MoS_2 a notable increase in the number of exposed molybdenum atoms surrounding the vacancies was observed, accompanied by a relatively lower oxidation state of Mo atoms and the presence of more unoccupied orbitals, collectively contributing to the optimization of the H adsorption/desorption equilibrium. Lee *et al.*[76] successfully synthesized a catalyst containing CrOx sub-nano domains through the migration of Cr cations at the interface of Co_9S_8/$CuCrS_2$. XPS analysis revealed a pronounced negative shift in the Co 2p peak of CrOx–Co_9S_8/$CuCrS_2$ compared to pristine Co_9S_8, indicating a strong electronic interaction

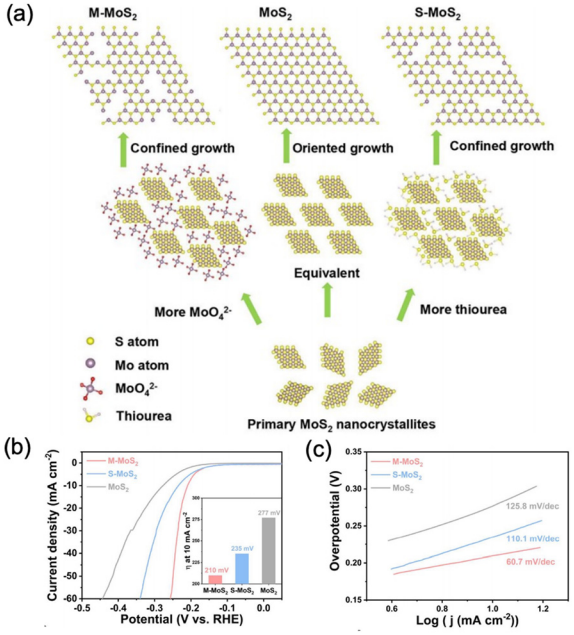

Fig. 6 (a) Schematic illustration for the synthesis of different vacancy states MoS_2. (b) Polarization curves, inset: overpotential at 10 mA cm^{-2}. (c) Tafel slopes in 0.5 M H_2SO_4.[75]

between Cr and Co metal centers, leading to electron transfer from Cr to Co. In 1.0 M phosphate buffer solution, the CrOx–Co_9S_8/$CuCrS_2$ catalyst exhibited remarkable HER activity, achieving an overpotential of only 37 mV at a current density of −10 mA cm^{-2}, with a low Tafel slope of 49 mV dec^{-1} and exhibiting good long-term stability. DFT calculations further elucidated that Cr oxide species effectively modulated the electronic structure by altering the atomic arrangement and connectivity within the Co_9S_8 framework, thereby optimizing the adsorption and desorption processes of hydrogen atoms (H*) on the catalyst surface.

Zou *et al.*[77] successfully developed a facile room-temperature synthesis method for the large-scale fabrication of heazlewoodite-phase $(Ni,Fe)_3S_2$ nanosheet arrays supported on nickel–iron foam (NFF). The electrode exhibited efficient and stable catalytic performance for HER and OER in alkaline media. Specifically, in a 30% KOH solution, the $(Ni,Fe)_3S_2$/NFF electrode delivered a HER overpotential of 168 mV and an OER overpotential of 241 mV at a current density of 100 mA cm^2. An alkaline electrolyzer constructed using $(Ni,Fe)_3S_2$/NFF electrodes as both the cathode and anode achieved a current density of 600 mA cm^{-2} at a voltage of just 1.93 V under conditions of 80 °C and 30% KOH electrolyte, and could operate stably for over 400 hours under these conditions. DFT calculations further revealed that the incorporation of Fe atoms not only significantly enhanced the activity of the existing catalytic sites in $(Ni,Fe)_3S_2$, but also converted originally inactive sites into active ones, thereby greatly improving its HER catalytic performance. Artero *et al.*[78] comprehensively reported three scalable synthesis methods that successfully fabricated bimetallic iron–molybdenum sulfide materials through microwave irradiation or thermal treatment within inert and reducing atmospheres. The results indicated that the

Table 3 A comparison of catalytic HER performances for the metal sulfide-based catalysts

Catalyst	Electrolysis test	Electrolyte	Current density (mA cm^{-2})	Overpotential (mV)	Tafel slope (mV dec^{-1})	Ref.
Cu NDs/Ni_3S_2 NTs-CFs	HER	1 M KOH	10	128	76.2	70
(Zn–)Co_9S_8@CF	HER	0.5 M H_2SO_4	10	273	85.2	72
		1 M KOH	10	278	114.4	
Co-1T-MoS_2-bpe	HER	1 M KOH	10	118	83	73
M-MoS_2	HER	0.5 M H_2SO_4	10	210	60.7	75
CrO_x–Co_9S_8/$CuCrS_2$	HER	1 M PBS	10	37	49	76
$(Ni,Fe)_3S_2$/NFF	HER	30% KOH	100	168	38.3	77
	OER	30% KOH	100	241	31.1	
FeMoS(mw)	HER	0.5 M H_2SO_4	10	140	57	78

amorphous FeMoS(mw) material obtained *via* the microwave synthesis route exhibited remarkably outstanding HER performance in acidic media, as evidenced by a low overpotential of 140 mV at a current density of 10 mA cm^{-2}. Subsequently, the research team assembled a proton exchange membrane electrolyzer single cell by employing FeMoS(mw) as the cathode catalyst in conjunction with iridium black as the anode catalyst. The performance of this electrolyzer was thoroughly tested under operating conditions at 80 °C. The test results revealed that the Ir/FeMoS(mw) electrolyzer required an additional voltage of approximately 300 mV at a current density of 0.5 A cm^{-2}, demonstrating competitive performance compared to conventional Pt-based catalysts.

In conclusion, sulfide-based electrocatalysts for HER represent a promising class of electrocatalysts with significant potential for widespread application. These catalysts exhibit unique physicochemical properties and exceptional electrocatalytic performance, establishing them as pivotal contributors to future hydrogen production efforts.[79]

The catalytic HER performances of various metal sulfide-based electrodes are compared in Table 3.

3.4 Metal selenide

Selenides, characterized by their distinctive electronic structure, significantly enhance electrocatalytic reactions. The synthesis of these catalysts employs a variety of methods, including hydrothermal and electrodeposition techniques. Furthermore, the catalytic performance can be optimized by modulating the raw material ratio during the synthesis process.

Feng *et al.*[80] successfully grew vertically oriented cobalt selenide ($Co_{0.85}Se$) nanosheets on graphene foil *via* an electrochemical exfoliation method. Subsequently, they employed a hydrothermal treatment technique to deposit NiFe layered double hydroxide (NiFe-LDH) onto the surface of the $Co_{0.85}Se$ nanosheets, thereby constructing a ternary composite material (EG/$Co_{0.85}Se$/NiFe-LDH). This three-dimensional composite material exhibits a high specific surface area of 156 m^2 g^{-1} and demonstrates excellent catalytic activity for the HER, with an overpotential of only −0.26 V at a current density of 10 mA cm^{-2}. In-depth studies reveal that interfacial covalent C–O···Co–Se bonds are formed within the EG/$Co_{0.85}Se$/NiFe-LDH composite material. This strong chemical coupling effect effectively optimizes the electronic structure, significantly reduces the charge transfer resistance, and consequently facilitates the rapid charge transfer process between $Co_{0.85}Se$ and graphene. Wang *et al.*[81] designed and prepared a novel Ru/Ni_3Se_2 composite material supported on nickel foam (NF) through hydrothermal reaction and wet chemical etching techniques. Notably, the loading amount of Ru on Ni_3Se_2 in this catalyst is only 2.34 wt%, which is significantly lower than that of most noble metal-based catalytic materials reported in previous literature. The research results indicate that the introduction of Ru markedly reduces the crystallinity of the Ni_3Se_2 material, thereby generating more lattice defects or edges. These unique structural features exhibit significant advantages in HER process, as they not only increase the number of active sites but also enhance the transfer efficiency of reactants. Furthermore, in-depth analysis reveals strong electronic interactions between Ru and Ni_3Se_2. Specifically, electrons flow from Ni and Se atoms to Ru atoms, leading to the redistribution of interface charges. This optimization of the electronic structure further enhances the electrocatalytic activity of the catalyst. DFT calculation results show that the d-band center of Ru/Ni_3Se_2 shifts slightly relative to that of Ni_3Se_2, which implies a weakened interaction between H and metal atoms. This change is of crucial importance for optimizing the ΔG_{H^*} and improving HER activity. Wang *et al.*[82] successfully synthesized a Co-doped selenide nickel composite ($NiSe_2$ and Ni_3Se_4) on nickel foam using metal–organic frameworks as precursors (Fig. 7a). The composite material exhibits effective catalytic activity for HER, achieving a current density of 10 mA cm^{-2} with an overpotential of merely 90 mV. Moreover, it demonstrates superior catalytic performance for OER, requiring an overpotential of only 275 mV to attain a current density of 30 mA cm^{-2}. Additionally, when employed as both cathode and anode in alkaline media for overall water splitting to achieve 10 mA cm^{-2}, it necessitates a voltage of only 1.6 V. Han *et al.*[83] anchored Pt single atoms onto nickel selenide enriched with cationic vacancies (NiSe-V) *via* a hydrothermal reaction followed by a wet-chemical impregnation method (Fig. 7b). This approach leveraged the low electron-density regions of NiSe-V to effectively trap and confine Pt atoms with high electron density, forming stable Pt–Se electronic bridges that facilitate rapid electron transport. Furthermore, the cationic vacancies in NiSe-V

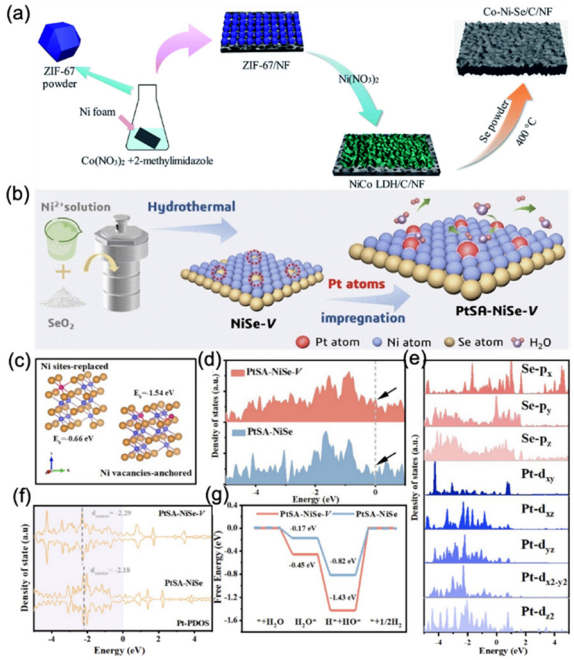

Fig. 7 (a) Illustration of the synthetic route of Co–Ni–Se/C/NF.[82] (b) Schematic illustration for the synthesis of PtSA-NiSe-V. (c) Calculated formation energies of replacing Ni sites and anchoring Ni vacancies of PtSA-NiSe-V. (d) Total density of state. (e) Partial density of state of Pt and Se atoms of the PtSA-NiSe-V structure. (f) Pt PDOS of PtSA-NiSe-V and PtSA-NiSe. (g) The free energy diagram for HER in alkaline solution for PtSA-NiSe-V and PtSA-NiSe.[83]

were effectively filled upon the anchoring of Pt single atoms, contributing to the structural stability during the HER process. As a result, the catalyst exhibited an extremely low overpotential of only 45 mV at a current density of 10 mA cm^{-2}, accompanied by excellent stability over 120 hours. DFT calculations revealed that the d-band center value of PtSA-NiSe-V is slightly lower than that of PtSA-NiSe, which helps weaken the Pt–H bond strength, thereby enhancing HER activity (Fig. 7c–g).

Guo *et al.*[84] employed a strategy combining crystal oriented growth and interface engineering to treat PtCo alloy nanosheets through a controlled local selenization method, successfully constructing two-dimensional $PtSe_2$/PtCo heterojunction nanosheets with high electrocatalytic activity. During the selenization process, nanopore structures were uniformly introduced into the nanosheets, a design that effectively facilitated mass transport in the electrocatalytic process. The prepared catalyst exhibited excellent HER electrocatalytic performance in acidic media. Specifically, when the current density reached 10 mA cm^{-2}, the HER overpotential was as low as 38 mV, and the Tafel slope was only 22 mV dec^{-1}. Furthermore, the catalyst possessed outstanding continuous and cycling stability. DFT calculations revealed that the polarization effect at the $PtSe_2$/PtCo heterojunction interface led to electron transfer from $PtSe_2$ to PtCo, thereby forming an internal electric field. This internal electric field not only enhanced the conductivity of the $PtSe_2$//PtCo heterojunction but also optimized the adsorption and desorption processes of H* (Fig. 8).

In summary, selenide-based catalysts exhibit high-efficiency performance in hydrogen evolution. Their design and synthesis methods are versatile, allowing for optimization and adjustment to meet specific application requirements. Particularly within the energy sector, especially in hydrogen energy, these catalysts possess significant potential for widespread applications.

The catalytic HER performances of various metal selenide-based electrodes are compared in Table 4.

3.5 Metal carbide

Carbide catalysts have demonstrated exceptional catalytic performance in the electrocatalytic HER. These catalysts typically exhibit excellent conductivity and chemical stability, rendering them ideal for application in HER. The catalytic mechanism of carbide catalysts primarily relies on the precise regulation of adsorption and dissociation capabilities of reaction intermediates to optimize the reaction pathway. Specifically, carbides possess a strong ability to adsorb and activate water molecules or hydrogen ions, thereby facilitating hydrogen gas production. Furthermore, carbides can be synergistically combined with other compounds, enhancing their catalytic activity through the formation of composite materials.

Wang *et al.*[85] synthesized vertically aligned porous pure-phase tungsten-based bimetallic carbide nanosheets (Co_6W_6-C@NC/CC) embedded within a nitrogen-doped carbon matrix on flexible carbon cloth, employing a MOF-derived method

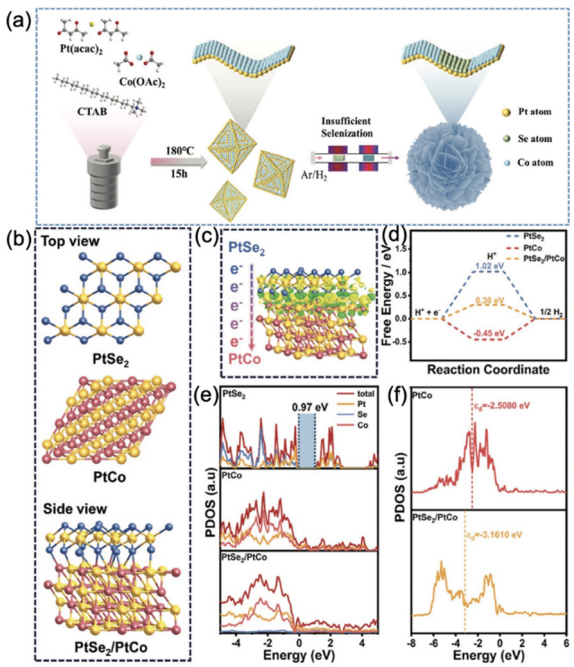

Fig. 8 (a) Schematic diagram of $PtSe_2$/PtCo catalyst synthesis. (b–f) DFT calculations for the $PtSe_2$/PtCo heqterojunction.[84]

Table 4 A comparison of catalytic HER performances for the metal selenide-based catalysts

Catalyst	Electrolysis test	Electrolyte	Current density (mA cm^{-2})	Overpotential (mV)	Tafel slope (mV dec^{-1})	Ref.
$Co_{0.85}Se$	HER	1 M KOH	20	260	—	80
	OER	1 M KOH	150(250)	270(280)	57	
Ru/Ni_3Se_2	HER	1 M KOH	10	24	45	81
	OER	1 M KOH	10	211	78	
Co–Ni–Se/C/NF	HER	1 M KOH	10	90	81	82
	OER	1 M KOH	30	275	63	
PtSA-NiSe-V	HER	1 M KOH	10	45	52	83
$PtSe_2$/PtCo	HER	0.5 M H_2SO_4	10	38	22	84

(Fig. 9a). The unique independent porous nanosheet structure of Co_6W_6C@NC/CC enhances contact between the electrolyte and active sites. Concurrently, the synergistic effect of cobalt and tungsten atoms effectively modulates the electronic structure, thereby optimizing hydrogen binding energy. Furthermore, the nitrogen-doped carbon matrix not only serves as a structural skeleton to enhance material stability but also improves conductivity, resulting in overpotentials of 59 mV and 110 mV at current densities of 10 mA cm^{-2} and 50 mA cm^{-2}, respectively (Fig. 9b–d).

Paul K. Chu *et al.*[86] synthesized a Mo_2C/VC heterojunction embedded in a graphitic carbon network composite (Mo_2C/VC@C) *via* magnesiothermic reduction using V_2MoO_8 as the precursor and $NaHCO_3$ as the carbon source. Within this composite, the VC and Mo_2C nanoparticles are intertwined, providing an enlarged interfacial area. The incoherent interfaces offer more defects and stronger interactions, leading to an increase in active sites for HER. As a result, the HER activity of Mo_2C/VC@C is significantly superior to that of Mo_2C@C, VC@C, and physically mixed Mo_2C@C/VC@C. Additionally, the three-dimensional carbon network exhibits remarkable mass and charge transfer capabilities, as well as high chemical stability, contributing to the conductivity and durability of Mo_2C/VC@C. DFT calculations reveal that the heterointerface of Mo_2C/VC modifies the electronic structures of Mo_2C and VC, reducing the binding energy with hydrogen, thereby enhancing the HER performance. Wang *et al.*[87] synthesized three-dimensional porous Co-doped β-Mo_2C spheres (Co_{50}-Mo_2C-12) through a multi-step process involving hydrothermal synthesis, carburization, and HCl etching (Fig. 10a). The results revealed that Co_{50}-Mo_2C-12 possesses abundant Mo vacancies, which are located at the edges of the molybdenum carbide surface. Additionally, lattice distortions, edge dislocations, and twin structures were observed in the material. The synergistic effect of Co doping and Mo vacancies increased the electron density near the Fermi level of β-Mo_2C, enriching electrons around the Mo atoms, thereby modulating the valence band structure and d-band center position of Mo_2C. Furthermore, changes in the d-band center of molybdenum carbide significantly influenced the adsorption–desorption equilibrium of H*, thereby enhancing its intrinsic activity, as shown in Fig. 10b and c.

Nicos Tagmatarchis *et al.*[88] successfully synthesized carbon dots (CDs) on carbon nanohorns (CNHs) through a simple hydrothermal method, thereby establishing a non-metallic all-carbon heterojunction structure (CDs/CNHs). The

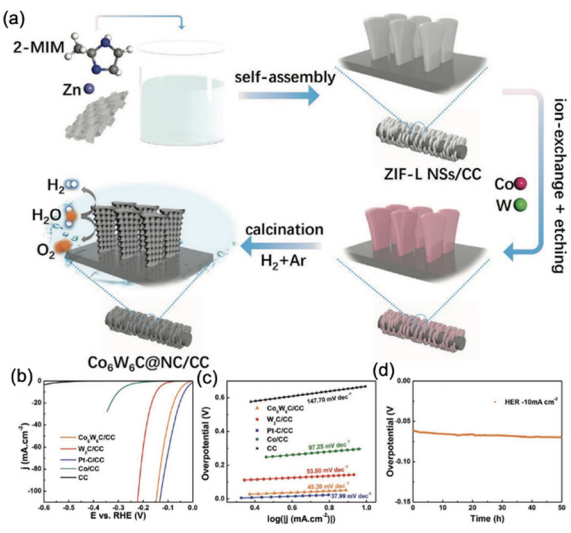

Fig. 9 (a) The synthesis procedure of Co_6W_6C@NC/CC. (b) Polarization curves, (c) Tafel slopes, (d) the long-time chronopotentiometry curve.[85]

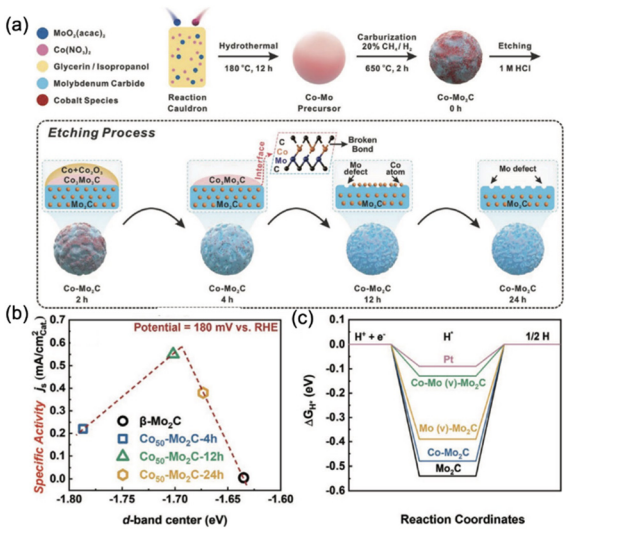

Fig. 10 (a) Schematic representation of the synthesis of Co-Mo_2C-t electrocatalyst. (b) Relationship between specific activity at 180 mV and d-band center for different catalysts, (c) free energies of H adsorption on different catalysts.[87]

distinctive three-dimensional porous architecture of the CNH not only offers enhanced conductive support for the *in situ* synthesis of CDs but also significantly improves charge transfer at the heterojunction interfaces, resulting in remarkable electrocatalytic activity. Zhang *et al.*[89] successfully synthesized an *in situ* nitrogen-doped carbon (N-C) substrate characterized by a high specific surface area and a porous structure rich in porosity through the pyrolysis of the ZIF-8 precursor. Subsequently, they incorporated boron (B), phosphorus (P), or sulfur (S) into the prepared N-C substrate *via* a two-step pyrolysis process under a nitrogen atmosphere, thereby producing BN-C, BPN-C, or BSN-C catalysts. In alkaline solution, the BSN-C catalyst exhibited superior performance for HER, achieving 10 mA cm^{-2} at an overpotential of 129.7 mV with a Tafel slope of 72.7 mV dec^{-1}.

Liu *et al.*[90] synthesized a heterostructured catalyst consisting of a nitrogen-doped tungsten carbide/tungsten metal interface (N-W_2C/W) on carbon fiber paper through a consecutive two-step method. This catalyst exhibited remarkable HER activity and stability over a full pH range. Theoretical calculations revealed that, in acidic media, the heterostructured interface in the N-W_2C/W catalyst facilitated a decrease in ΔG_{H^*}, making it easier for adsorbed hydrogen atoms on the surface to desorb as H_2. In alkaline and neutral media, H_2O was first adsorbed onto the W atoms at the N-W_2C/W interface. During the subsequent water dissociation process, due to the larger ΔG_{H^*} of W, H* was more likely to adsorb onto the W atoms of the metallic W in N-W_2C/W, while OH* was more likely to adsorb onto the W atoms of N-W_2C. N-W_2C/W exhibited strong adsorption of both initial H_2O* and final H + OH states, which favored the Volmer reaction and contributed to the enhanced activity of the catalyst in alkaline and neutral media. Therefore, the presence of the N-W_2C/W interface provided synergistic adsorption sites, thereby improving the water dissociation ability. Yang *et al.*[91] proposed a crystal phase engineering strategy to tune the interfacial interaction by loading Ru clusters onto precisely prepared cubic and hexagonal molybdenum carbides (α-MoC/β-Mo_2C) supports (Fig. 11a). Spectroscopic analysis revealed that Ru exhibited a lower valence state on β-Mo_2C compared to α-MoC, indicating that Ru could transfer more electrons from the support, thereby promoting the interfacial interaction between Ru and molybdenum carbide and enhancing the HER activity. The results demonstrated that the crystal phase structure of the support had a significant impact on HER activity, with β-Mo_2C exhibiting the highest HER activity as the support.

Cui *et al.*[92] delved into the influence of molybdenum carbide (Mo_2C) oxidation gradient on HER activity by finely tuning the surface oxidation state of the Mo_2C catalyst. The results revealed that the Mo_2C catalyst modified with slight oxidation exhibited the most superior HER activity. *In situ* and quasi-*in situ* XPS measurements further confirmed that

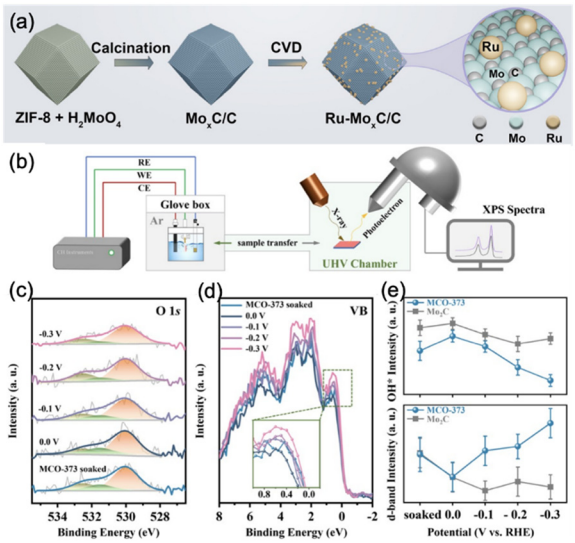

Fig. 11 (a) Schematic illustration for the synthesis process of Ru-Mo_xC.[91] (b) Schematic illustration of the quasi *in situ* alkaline HER experimental setup. (c and d) Quasi *in situ* XPS spectra of (c) O 1s and (d) valence band for MCO-373 sample soaked in KOH. (e) Intensity of surface adsorbed hydroxyl and Mo 4d for Mo_2C and MCO-373 samples.[92]

moderately oxidized Mo_2C not only effectively facilitated the cleavage of H–OH bonds during the water activation process but also significantly accelerated the desorption kinetics of the generated OH* intermediates, thereby comprehensively enhancing the overall reaction rate of HER in alkaline environments (Fig. 11b–e). This study provides a novel approach for the design and development of low-cost, high-efficiency oxygen-modified molybdenum carbide catalysts. Non-active metals can also modulate the electronic structure of TMCs (transition metal carbides). Recently, Zheng *et al.*[93] found that Al doping can induce electron redistribution on the surface of vanadium carbide, forming electron-rich C active sites, thereby significantly reducing ΔG_{H^*} and enhancing HER performance.

The rapid advancement of renewable and hydrogen energy technologies has highlighted the significant potential for diverse applications in the research and development of non-metallic catalysts for HER. Future directions include the design of more efficient, stable, and cost-effective non-metallic catalysts, thereby providing substantial support for the advancement of water electrolysis technology. Non-metallic catalysts constitute a distinct class with unique advantages and opportunities. A thorough understanding of their various types, mechanisms of action, benefits, challenges, and current research progress is crucial to optimizing their utilization and fostering further development. This will facilitate improvements in and applications of water electrolysis hydrogen production technology.

The catalytic HER performances of various metal carbide-based electrodes are compared in Table 5.

Table 5 A comparison of catalytic HER performances for the metal carbide-based catalysts

Catalyst	Electrolysis test	Electrolyte	Current density (mA cm^{-2})	Overpotential (mV)	Tafel slope (mV dec^{-1})	Ref.
Co_6W_6C@NC/CC	HER	1 M KOH	10(50)	59(110)	45.39	85
	OER	1 M KOH	10(50)	286(326)	53.96	
Mo_2C/VC@C	HER	0.5 M H_2SO_4	10	122	43.8	86
β-Mo_2C	HER	1 M $HClO_4$	10	125	100.28	87
			50	180		
CDs/CNHs	HER	0.5 M H_2SO_4	10	190	97	88
BSN-C	HER	1 M KOH	10	129.7	72.7	89
N-W_2C/W	HER	0.5 M H_2SO_4	10	90	33.6	90
		1 M KOH	10	82	49.2	
		1 M PBS	10	90	54	
Ru–Mo_2C/C	HER	0.5 M H_2SO_4	10	18	32	91
Al-VC@C/NF	HER	0.5 M H_2SO_4	10	58	45	93
		1 M KOH	10	97	73	
Mo_2C	HER	1 M KOH	10	205	78	92

3.6 Metal phosphide

In recent years, transition metal phosphides (TMPs) have attracted considerable attention in HER due to their exceptional performance. The phosphorus atoms within TMPs possess strong electronegativity, effectively drawing electrons from metal atoms and acting as proton acceptors, thereby facilitating the HER process. The catalytic efficacy of phosphide materials is influenced by various factors, including morphology, size, and surface characteristics. By carefully designing and synthesizing phosphide materials with tailored morphologies and structures, their catalytic performance can be further optimized. Moreover, researchers have successfully enhanced the catalytic activity of phosphide catalysts through strategies such as doping and alloying.

Lee *et al.*[94] successfully synthesized Ir_2P cluster-decorated Ru_2P hollow nanotubes (c-RP/IP HNTs) *via* an ion exchange strategy, enabling the synergistic interaction between Ru_2P and Ir_2P (Fig. 12a). The c-RP/IP HNTs catalyst exhibited remarkable HER performance under alkaline conditions, achieving a current density of 10 mA cm^{-2} at an overpotential of 23.2 mV with a Tafel slope of 30.7 mV dec^{-1}, outperforming commercial Pt/C and Ru/C catalysts. In practical AEMWE single-cell tests, the c-RP/IP HNTs catalyst demonstrated a current density of 12.23 A cm^{-2} at 2.0 V, surpassing the performance of commercial Pt/C catalyst. XPS analysis revealed that both Ru and Ir exist in the form of metal phosphides, with electron transfer from Ru_2P to Ir_2P, facilitating the HER process. DFT calculations identified Ru(4) and Ir(3) sites as the active sites for HER, enabling a rapid cascade reaction through the hydrogen spillover effect.

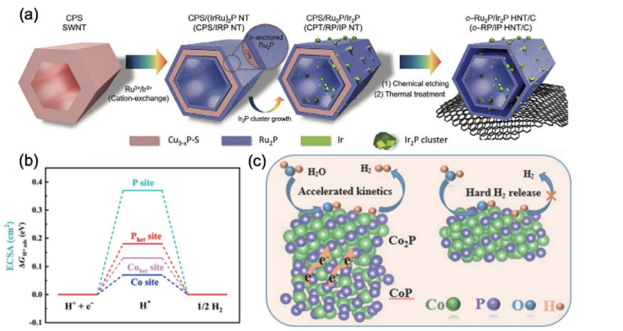

Fig. 12 (a) Schematic illustration of the synthesis of c-RP/IP HNTs.[94] (b) DFT calculation results. (c) Illustration of activation of P site by heterojunction accelerates hydrogen release mechanism.[95]

Zhang *et al.*[95] successfully synthesized well-crystallized Co_2P/CoP heterojunction nanoparticles with intimate interface contact through a two-step method involving pyrolysis and phosphidation. Compared to single-phase Co_2P and CoP catalysts, the Co_2P/CoP heterojunction material exhibits superior HER activity, faster reaction kinetics, and higher electron transfer efficiency. The interaction between the electronic structures within the Co_2P/CoP heterojunction results in the preferential migration of free electrons from Co sites to P sites, ultimately accumulating at the P sites. This redistribution of electrons facilitates the adsorption and desorption of hydrogen intermediates at the P sites, thereby enhancing the activity of the P sites. DFT theoretical calculations reveal that the hydrogen adsorption barrier at the P sites is significantly reduced upon the formation of the heterojunction, further confirming that the heterojunction activates the P sites, leading to an increase in active sites and improved reaction kinetics of the material (Fig. 12b and c). Zhao *et al.*[96] introduced a comprehensive urea-modulated hydrothermal phosphorization synthesis method to fabricate multilevel CoMnP/Ni_2P nanosheet arrays (CoMnP/Ni_2P/NF) on highly conductive nickel foam, which exhibit superhydrophilicity and superoleophobicity properties. Recognized as an exceptional non-precious bifunctional electrocatalyst, CoMnP/Ni_2P/NF demonstrated significant potential in the overall water splitting reaction. The optimized CoMnP/Ni_2P/NF electrocatalyst achieved overpotentials of 84 mV and 108 mV at 10 mA cm^{-2} for HER in 0.5 M H_2SO_4 and 1 M KOH, respectively, along with overpotentials of 165 mV and 209 mV for OER in the same electrolytes. The superior electrocatalytic performance can be attributed to the synergistic catalytic effect of CoP–MnP for HER and CoOOH–MnOOH for OER, significantly enhancing the intrinsic activity of the catalyst. Furthermore, its unique

multilevel structure effectively increased the electrochemically active surface area while its superhydrophilicity and superoleophobicity facilitated rapid bubble detachment as well as efficient electron and mass transfer.

Kuang *et al.*[97] successfully synthesized porous molybdenum tungsten phosphide (Mo–W–P) composite nanosheets through the *in situ* phosphorization of molybdenum tungsten oxide (Mo–W–O) composite nanowires, which were grown on carbon cloth. The Mo–W–P composite exhibits a modest overpotential of 138 mV to achieve a high current density of 100 mA cm^{-2} in 0.5 M H_2SO_4, with a Tafel slope of 52 mV dec^{-1}. This performance significantly surpasses that of individual MoP nanosheets and WP_2 nanorods. The superior catalytic performance for HER exhibited by Mo–W–P is primarily attributed to the three-dimensional conductive structure provided by nickel foam, the porous nanosheet architecture of Mo–W–P, and the strong synergistic interaction between W and Mo atoms within the composite. These findings suggest that meticulous control over the morphology and composition of electrocatalysts can effectively facilitate the preparation of efficient composite electrocatalysts. Liu *et al.*[98] successfully transformed Ni–WO_3 NS/CC into Ni–WP_2 NS/CC through a phosphating treatment process. XPS results revealed that Ni doping induces partial electron transfer from W to Ni. Furthermore, there exists a stronger electronic interaction between the dopant Ni and WP_2, facilitating the accumulation of electrons at the P sites, which participate more effectively in the catalytic reaction, thereby significantly enhancing the performance of HER. After optimization, the Ni-doped WP_2NS/CC material exhibited an increased number of active sites and a decreased charge transfer resistance. Consequently, compared to pristine WP_2, the material demonstrated superior HER activity and stability (Fig. 13). DFT calculations further corroborated that the addition of Ni effectively modulated the electronic structure of WP_2. Specifically, Ni doping shifted the d-band center of WP_2 away from the Fermi level, which, according to the d-band theory, aids in weakening the adsorption strength of hydrogen on the catalyst surface, ultimately enhancing the HER activity.

Mu *et al.*[99] utilized Prussian blue analogues as precursors to synthesize transition metal phosphides with ultra-low Ru loading (Ru–MnFeP/NF) through doping and phosphating processes. Ru–MnFeP/NF exhibits a unique nanosheet structure, characterized by a high specific surface area and abundant active sites, which facilitates electron transfer and bubble release. In 1 M KOH solution, Ru–MnFeP/NF demonstrates excellent HER performance, achieving an overpotential of 35 mV at a current density of 10 mA cm^{-2}, which is lower than the 39 mV of commercial Pt/C catalysts, with a Tafel slope of 36 mV dec^{-1}. DFT calculations indicate that Ru metal loaded with Fe_2P or Mn_2P exhibits reduced adsorption of *H, and changes occur in the electronic structure between Ru and the phosphide. Yu *et al.*[100] selected nickel foam as the substrate material and successfully grew

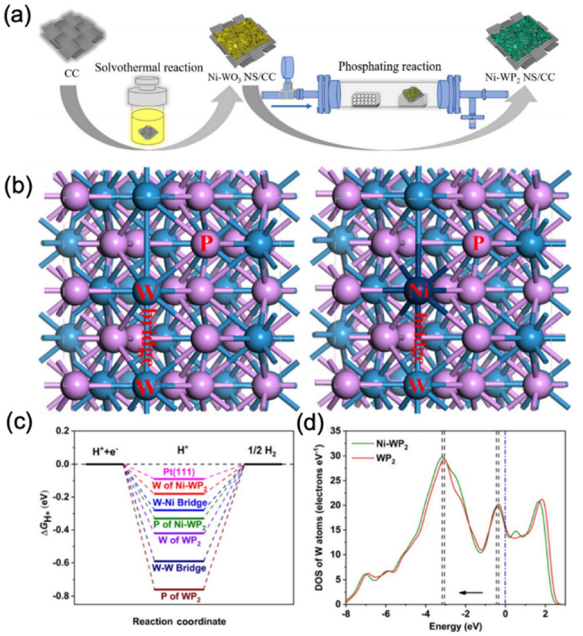

Fig. 13 (a) Schematic illustration of the fabrication of Ni–WP_2 NS/CC catalysts. (b) The slab models of WP_2 and Ni–WP_2 used for geometry optimization. (c) The calculated hydrogen adsorption Gibbs free energy diagram for WP_2 and Ni–WP_2 on different sites. (d) The d-orbital partial density of states (d-DOS) of W atoms, the vertical blue dash-dot line shows the position of the Fermi level.[98]

$NiCo_2O_4$ nanorod arrays on the surface of the nickel foam *via* hydrothermal synthesis. Subsequently, they employed electrochemical deposition to deposit $Co(OH)_2$ nanosheets on the $NiCo_2O_4$ nanorod arrays and further subjected the resulting material to nitridation and phosphatization treatments, ultimately preparing the N–Co_2P/$NiCo_2O_4$/NF composite catalyst. The three-dimensional porous hierarchical structure of this catalyst not only significantly increases the electrochemical active surface area but also effectively facilitates electron transfer and bubble release. In alkaline media, the N–Co_2P/$NiCo_2O_4$/NF composite catalyst exhibits excellent HER performance, with an overpotential of only 58 mV and a Tafel slope as low as 75 mV dec^{-1} at a current density of 10 mA cm^2. DFT calculations reveal that nitrogen doping can effectively modulate the electronic structure of Co_2P, lowering its d-band center position, thereby weakening the adsorption strength of hydrogen on the catalyst surface, optimizing the hydrogen adsorption free energy, and ultimately enhancing HER activity. Min *et al.*[101] effectively regulated the lattice tensile strain of nickel cobalt phosphide (NiCoP) through a ruthenium (Ru) doping strategy and successfully anchored it onto carbonized wood (CW), preparing a Ru–NiCoP/CW catalyst with excellent HER performance. In 1.0 M KOH solution, the catalyst exhibited an extremely low overpotential (−25 mV) and a small Tafel slope (60 mV dec^{-1}) at a current density of 10 mA cm^{-2}, outperforming most reported HER electrocatalysts. XPS analysis revealed that the doping of Ru not only induced lattice strain but also significantly optimized the electronic

Table 6 A comparison of catalytic HER performances for the metal phosphide-based catalysts

Catalyst	Electrolysis test	Electrolyte	Current density (mA cm^{-2})	Overpotential (mV)	Tafel slope (mV dec^{-1})	Ref.
c-RP/IP HNT/C	HER	1 M KOH	10	23.3	30.7	94
CoMnP/Ni_2P/NF	HER	1 M KOH	10	108	87	96
		0.5 M H_2SO_4	10	84	57	
	OER	1 M KOH	10	209	49	
		0.5 M H_2SO_4	10	165	76	
Co_2P/CoP-350	HER	1 M KOH	10	121	84.9	95
Mo–W–P/CC	HER	0.5 M H_2SO_4	100	138	52	97
Ni–WP_2 NS/CC	HER	0.5 M H_2SO_4	10	110	65	98
Ru–MnFeP/NF	HER	1 M KOH	10	35	36	99
	OER	1 M KOH	20	191	69	
N–Co_2P/$NiCo_2O_4$/NF	HER	1 M KOH	10	58	75	100
Ru–NiCoP/CW	HER	1 M KOH	10	25	60	101

structure of the catalyst, enhancing the electron transfer efficiency between the metal and phosphorus elements.

While phosphide catalysts exhibit commendable efficacy in HER, their practical implementation is hindered by several challenges, particularly regarding cost and stability. Therefore, it is essential for future research efforts to continuously develop innovative preparation methodologies and explore optimization strategies aimed at enhancing the performance of phosphide catalysts. Such advancements will effectively reduce costs, thereby promoting their widespread application in hydrogen energy production.

The catalytic HER performances of various metal phosphide-based electrodes are compared in Table 6.

3.7 Metal nitride

Nitride catalysts exploit the unique properties and structures of nitrides to accelerate the reduction process of hydrogen ions, thereby enhancing both the efficiency and yield of HER. Among nitride catalysts, transition metal nitrides (TMNs) such as titanium nitride (TiN) and molybdenum nitride (MoN) have garnered considerable attention due to their excellent conductivity, stability, and corrosion resistance. These nitride catalysts provide a multitude of active sites for HER, effectively facilitating the adsorption and dissociation of hydrogen ions while accelerating hydrogen gas production. However, nitride catalysts also encounter several challenges in practical applications. Firstly, their catalytic performance may be influenced by preparation methods and conditions, necessitating optimization of these processes to enhance catalyst performance. Secondly, active sites on nitride catalysts can be disrupted by substances such as hydroxide ions, adversely affecting their catalytic activity. Therefore, a comprehensive investigation into the characteristics of the catalyst's active sites and the underlying reaction mechanisms is essential for further optimizing its catalytic performance.

Duan *et al.*[102] successfully transformed NiFe-layered double hydroxide (LDH) into a porous nanoplate array of Fe_2Ni_2N under an NH_3 atmosphere. The bifunctional catalyst demonstrated exceptional overall water splitting activity in alkaline media. Due to its unique material and structural characteristics, Fe_2Ni_2N nanoplate array electrode exhibited a HER onset overpotential of 110 mV, an OER onset overpotential of 200 mV, with a Tafel slope of 101 mV dec^{-1} for HER and a Tafel slope of 34 mV dec^{-1} for OER. Furthermore, it displayed excellent electrochemical durability. The catalyst can be directly employed at both the anode and cathode, effectively facilitating the complete electrocatalytic water splitting reaction. Yu *et al.*[103] designed and investigated a three-dimensional core–shell structured catalyst (NiMoN@NiFeN), which consists of NiFeN nanoparticles uniformly decorated on NiMoN nanorods supported on nickel foam (Fig. 14a–d). In 1 M KOH electrolyte, this catalyst exhibited excellent HER activity, achieving current densities of 100 mA cm^{-2} and 500 mA cm^{-2} at overpotentials of 56 mV and 127 mV, respectively. Furthermore, by employing the NiMoN@NiFeN catalyst as the anode and the NiMoN catalyst as the cathode, a two-electrode seawater electrolyzer was assembled. At an

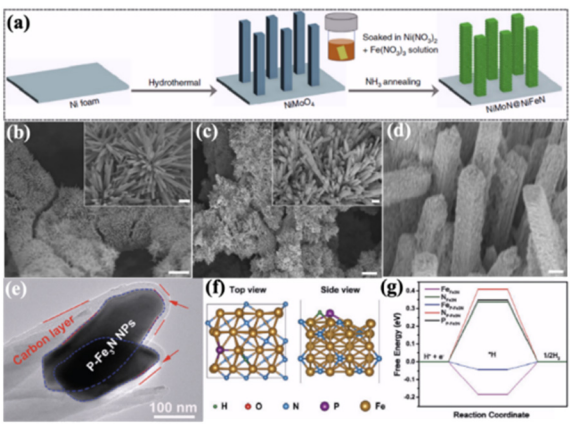

Fig. 14 (a) Schematic illustration of the synthesis procedures for the self-supported 3D core–shell NiMoN@NiFeN catalyst. (b) Low magnification SEM image of NiMoN, and inset: high magnification SEM image. (c) Low magnification SEM image of NiMoN@NiFeN, and inset: high magnification SEM image. (d) High magnification SEM image of NiMoN@NiFeN.[103] (e) TEM image of the P-Fe_3N@NC NSs/IF. (f) Top and side views of schematically atomic models showing P-Fe_3N with H adsorbed on Fe sites. (g) HER free energy diagram for different models on pristine and P-doped Fe_3N.[105]

operating temperature of 60 °C, this electrolyzer required voltages of 1.608 V and 1.709 V to reach current densities of 500 mA cm^{-2} and 1000 mA cm^{-2}, respectively, setting a new record in the field of seawater electrolysis. Yu *et al.*[104] successfully synthesized a series of high-performance transition metal phosphide/nitride heterogeneous electrocatalysts ($Fe_{2-2x}Co_{2x}P/Ni_3N$) through the *in situ* growth of highly dispersed iron-rich bimetallic phosphide nanoparticles on porous, highly conductive Ni_3N supports. These catalysts exhibited exceptional bifunctional catalytic activity for water splitting in alkaline seawater. Notably, $(Fe_{0.74}Co_{0.26})_2P/Ni_3N$ electrocatalyst achieved current densities of 100 mA cm^{-2} for both HER and OER at overpotentials of only 1 13 mV and 212 mV under 1 M KOH condition, respectively. Zhou *et al.*[105] utilized *Saccharomyces cerevisiae* as sources of carbon, nitrogen, and phosphorus to *in situ* grow phosphorus-doped iron nitride nanoparticles encapsulated within nitrogen-doped carbon nanosheets (P-Fe_3N@NC NSs/IF) on an iron foam substrate through a high-temperature carbonization process. Under alkaline conditions, the P-Fe_3N@NC NSs/IF electrode exhibited excellent performance for HER, achieving 10 mA cm^{-1} at an overpotential of 102 mV, along with good stability. DFT calculations revealed that the Fe sites in P-Fe_3N serve as the active centers, and the doping of N and P effectively modulates the hydrogen binding strength, enhancing the catalytic capability for water splitting (Fig. 14e–g).

Hu *et al.*[106] employed a slow etching and *in situ* co-precipitation technique to meticulously design and synthesize a $CoMoO_4{\cdot}xH_2O/NiMoO_4{\cdot}xH_2O$ heterostructured precursor on a nickel foam substrate. Subsequently, this precursor was subjected to high-temperature nitridation at 800 °C, successfully yielding a ternary nitride heterostructured catalyst (Co_3Mo_3N/Ni_3Mo_3N). The Co_3Mo_3N/Ni_3Mo_3N catalyst is rich in heterogeneous interfaces, where electron transfer at the heterointerfaces effectively optimizes the electronic structures of Co and Mo atoms, making Mo atoms the primary sites for water adsorption and Co atoms the sites for hydrogen adsorption, thereby significantly accelerating the kinetics of HER. DFT calculations reveal that Co_3Mo_3N/Ni_3Mo_3N exhibits a low water dissociation energy barrier and a more favorable hydrogen adsorption energy. Consequently, the catalyst demonstrates excellent HER performance. Specifically, in alkaline and neutral environments, at a current density of 10 mA cm^{-2}, Co_3Mo_3N/Ni_3Mo_3N exhibits low overpotentials of 36 mV and 58 mV, respectively. Wang *et al.*[107] innovatively proposed a synthesis method employing high-temperature shock (HTS) technique to load sub-2-nanometer ruthenium nanoclusters (HTS-Ru-NCs) onto titanium nitride (TiN) supports. In alkaline solutions, the HTS-Ru-NCs/TiN catalyst exhibited outstanding electrocatalytic activity for HER, with overpotentials of 16.3 mV and 86.6 mV required to achieve current densities of 10 mA cm^2 and 100 mA cm^2, respectively. Furthermore, this study successfully constructed an alkaline water electrolyzer and an anion exchange membrane water electrolyzer, both utilizing HTS-Ru-NCs/TiN as the cathode and NiFeOx as the anode, which were capable of delivering high current densities at low voltages. By employing *ab initio* molecular dynamics simulations, this study deeply elucidated the synergistic mechanism exhibited by Ru NCs and the TiN support at the interface. The simulation results clearly demonstrated that water molecules located at the interface could undergo unobstructed adsorption and dissociation processes, thereby significantly promoting the kinetics of the HER.

Luo *et al.*[108] successfully designed and prepared a highly efficient and stable Ru NPs/TiN HER catalyst through a multi-step synthesis method (Fig. 15a). Under alkaline conditions, the Ru NPs/TiN catalyst exhibits outstanding HER performance, achieving a current density of 100 mA cm^2 at an overpotential of only 73 mV, with a mass activity (20 A mg^{-1} Ru) significantly higher than that of commercial 20% Pt/C and 5% Ru/C catalysts. DFT calculations reveal a strong affinity between the Ru nanoparticles and the TiN support, with metal–support charge transfer effectively reducing the hydrogen adsorption energy on the Ru surface, thereby enhancing HER activity. Furthermore, an anion exchange membrane electrolyzer was successfully assembled using Ru NPs/TiN as the cathode catalyst and $NiMoFeO_x$/NF as the anode catalyst. The electrolyzer exhibits efficient water electrolysis performance under operating conditions of 80 °C and 1 bar, and demonstrates stable voltage with no significant fluctuations during prolonged operation (over 1000 hours), indicating promising industrial application prospects (Fig. 15b–e).

In conclusion, nitride-based hydrogen evolution catalysts demonstrate significant potential in the field of HER. However, their fabrication processes and catalytic performance require further optimization. Future research

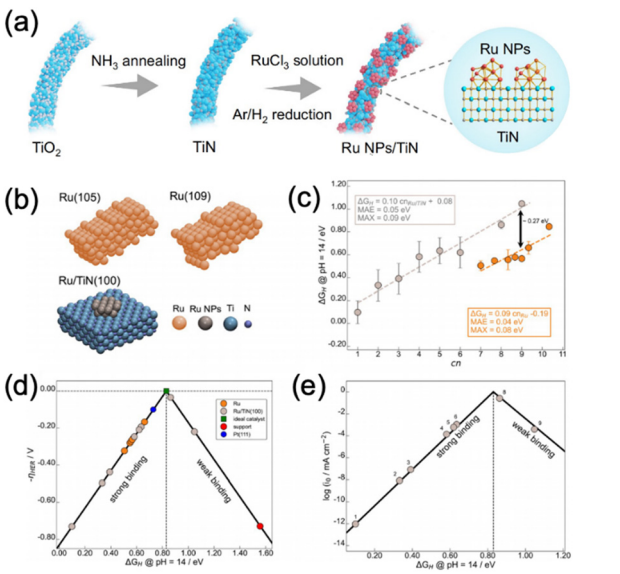

Fig. 15 (a) Schematics illustration for the synthesis of Ru NPs/TiN. (b) The pure, extended Ru surfaces and an exemplary Ru NP supported on TiN(100). (c) Relationships between the hydrogen adsorption energies (ΔG_H) and the coordination numbers (cn) of sites at Ru NPs (gray) and pure Ru (orange), along with their linear fits. (d) Thermodynamic volcano plot of the HER overpotential as a function of ΔG_H for sites on pure and supported Ru. (e) HER volcano plot for TiN(100)-supported Ru NPs built upon the experimental exchange current density of Ru/TiN(100).[108]

Table 7 A comparison of catalytic HER performances for the metal nitride-based catalysts

Catalyst	Electrolysis test	Electrolyte	Currentdensity (mA cm^{-2})	Overpotential (mV)	Tafel slope (mV dec^{-1})	Ref.
Fe_2Ni_2N	HER	1 M KOH	10	180	101	102
	OER	1 M KOH	—	—	34	
Ni_2Mo_3N/NF	HER	1 M KOH	100(500)	56 (127)	45.6	103
	OER	1 M KOH	100(500)	277 (337)	58.6	
$Fe_{2-2x}Co_{2x}P/Ni_3N$	HER	1 M KOH	100	113	31.8	104
	OER	1 M KOH	100	212	45.5	
P-Fe_3N@NC NSs/IF	HER	1 M KOH	10	102	68.59	105
	OER	1 M KOH	10	270	89.72	
Co_3Mo_3N/Ni_3Mo_3N	HER	1 M KOH	10(100)	36(130)	53	106
		1 M PBS	10(100)	58(245)	87.3	
HTS-Ru-NCs/TiN	HER	1 M KOH	10	16.3	36.0	107
Ru NPs/TiN	HER	1 M KOH	100	73	41.4	108

will focus on developing novel and efficient nitride hydrogen evolution catalysts, with particular emphasis on elucidating their catalytic mechanisms and reaction kinetics. Such efforts aim to enhance the proliferation and practical application of hydrogen energy technologies.

The catalytic HER performances of various metal nitride-based electrodes are compared in Table 7.

3.8 Metal boride

Boride catalysts, a unique category of catalysts, play a pivotal role in HER. For instance, metal borides may exhibit record-breaking intrinsic activity under acidic conditions, surpassing even that of commercial Pt/C catalysts. Notably, palladium diboride (Pd_2B) has been both theoretically and experimentally validated as an optimal candidate material. A novel method for synthesizing Pd_2B crystals *via* solvothermal synthesis has demonstrated its exceptional activity and high stability under intensely acidic conditions. This characteristic of Pd_2B primarily stems from its stable metallic bulk boride structure, particularly the hexagonal close-packed (hcp) structured Pd_2B phase.

Liu *et al.*[109] successfully synthesized a Pd_2B catalyst with a hexagonal close-packed (hcp) structure, high surface area, high catalytic activity, and high stability through a facile solvothermal method, using Pd(II)-acetylacetonate as the precursor for the metal boride and dimethylamine borane as the boron source. The catalyst exhibited a low overpotential of 15.3 mV at a current density of 10 mA cm^{-2}, along with a Tafel slope of merely 22.5 mV dec^{-1}, demonstrating significantly superior catalytic activity and stability compared to traditional Pt/C catalysts. DFT calculations revealed that the insertion of B atoms into the Pd lattice is a slow process, but can be markedly accelerated through a layered face-centered cubic (fcc) to hcp phase transition. Furthermore, the high HER activity of the Pd_2B catalyst is primarily attributed to the presence of subsurface B atoms and the lattice expansion upon the formation of the hcp lattice (Fig. 16a and b). These factors collectively contribute to the reduction of the H adsorption free energy, facilitating the H–H coupling reaction and thus significantly enhancing the HER activity. The research by Zou *et al.*[110] reveals that α-MoB_2, containing borophene-like subunits, not only exhibits catalytic activity at its edge sites but also at its basal plane sites, offering the possibility of providing a higher density of catalytically active sites. Through DFT calculations, the researchers found that the Mo-terminated (001) and (100) surfaces of α-MoB_2 can maintain a near-zero hydrogen adsorption free energy (ΔG_{H^*}) across a range of hydrogen coverages from low to high, indicating the material's significant activity for the HER. Furthermore, α-MoB_2 is capable of achieving a current density of 1000 mA cm^{-2} under a relatively small overpotential (334 mV), demonstrating its potential for practical applications. Do-Heyoung Kim *et al.*[111] designed and synthesized an electrocatalyst (P-NCB) exhibiting excellent activity for both HER and OER by introducing trace amounts of phosphorus into a NiCoB compound (NCB). In the P-NCB catalyst, cobalt and boron atoms serve as active catalytic sites, while nickel atoms help regulate the electronic structure of the material. Meanwhile, phosphorus doping plays a crucial role in optimizing HER performance, with boron acting as a bridge between metals and nonmetals. The water splitting

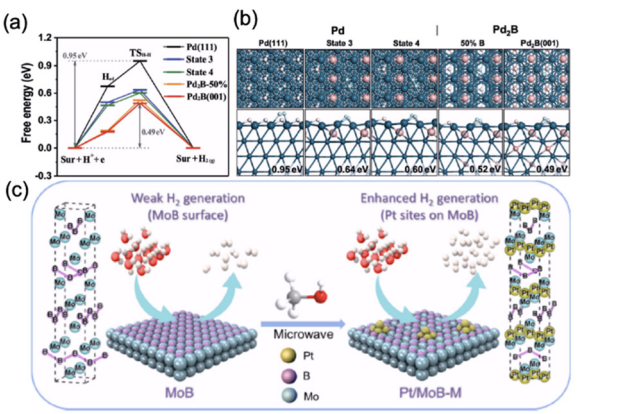

Fig. 16 (a) The free energy reaction profiles of H–H coupling on different surfaces. (b) The structures of the transition states. Both the top and the side views of each TS are shown.[109] (c) Schematic diagram of the synthesis of Pt/MoB-M.[113]

performance of P-NCB benefits from the synergistic effects of these elements, which lower the reaction barriers for both HER and OER. This metal-quasi-metal-nonmetal P-NCB electrocatalyst presents opportunities for developing more efficient bifunctional electrocatalysts in the future and opens new avenues for commercial energy conversion devices. Chen *et al.*[112] synthesized a Ni_xB/f-MWCNT composite material by anchoring ultrathin nickel boride (Ni_xB) sheets onto the surface of functionalized small-diameter multiwalled carbon nanotubes (f-MWCNTs). The electrochemical active surface area and charge transfer resistance of Ni_xB/f-MWCNT composite were found to be 3.4 times greater and 0.24 times lower than those of Ni_xB nanosheets, respectively. The Ni_xB/f-MWCNT exhibited superior catalytic activity and stability in both HER and OER. X-ray photoelectron spectroscopy reveals that Ni_xB exhibits a strong chemical coupling with f-MWCNTs, leading to the formation of highly active NiOOH/Ni_xBand $Ni(OH)_2/Ni_xB$ heterojunctions, which is an important reason for the excellent catalytic activity of Ni_xB/f-MWCNT. Wang *et al.* selected MoB as the support and successfully anchored Pt nanoclusters onto it through an innovative microwave-assisted method, with precise control over different solvents. This resulted in the fabrication of a highly efficient Pt/MoB catalyst (Fig. 16c). In-depth studies revealed that methanol played a crucial role in the catalyst synthesis process, effectively facilitating the uniform dispersion of Pt on the MoB support and consequently enhancing the electron transfer rate significantly. In a 0.5 M H_2SO_4 electrolyte, the prepared Pt/MoB-M catalyst exhibited an overpotential of merely 13 mV at a current density of 10 mA cm^{-2}, with a Tafel slope of 24 mV dec^{-1}. At an overpotential of 50 mV, the mass activity reached as high as 10.06 A mg^{-1} Pt. Notably, the strong interaction formed between Pt and the MoB support optimized the electronic structure of the catalyst, thereby greatly improving its HER activity. Furthermore, the presence of boron vacancies in the MoB support also positively contributed to the dispersion and stability of Pt.[113]

Despite the advantages of boride-based hydrogen evolution catalysts, their practical implementation is still hindered by factors such as cost and long-term stability. Therefore, future research efforts should focus on strategies to address these limitations, thereby enhancing the feasibility of large-scale applications.

The catalytic HER performances of various metal boride-based electrodes are compared in Table 8.

3.9 Single-atom catalysts

Single-atom catalysts (SACs) represent a category of catalysts in which catalytically active metal atoms are individually dispersed on supports, achieving a maximum atomic utilization efficiency of 100%. The unique electronic structure and unsaturated coordination environment of the single-atom active centers contribute significantly to enhancing the catalytic activity in various reactions. Furthermore, a strong interaction typically occurs between the active metal single atoms and the support, and the properties of the support can profoundly influence the chemical state and coordination structure of the metal single atoms, ultimately impacting the catalytic performance of the SACs.

Liu *et al.*[114] conducted an in-depth investigation into a series of single-atom electrocatalyst systems (TM/N_4C, where TM represents 3d, 4d, or 5d metals) using *ab initio* molecular dynamics simulations and free energy calculations. They discovered that a strong charge–dipole interaction exists between the negatively charged H* intermediate and interfacial H_2O molecules. This interaction is capable of altering the transition state pathway of the acidic Volmer reaction and notably elevating its kinetic barrier. Wang *et al.*[115] successfully synthesized a PtSA-NiO/Ni catalyst by employing a cyclic voltammetric electroreduction strategy, which involves the deposition of single-atom Pt onto the surface of NiO/Ni heterojunction supported on silver nanowires (Fig. 17a). In the PtSA-NiO/Ni catalyst, the metallic Ni sites facilitate the adsorption and conversion of hydrogen (H), while the oxygen vacancy-modified NiO sites promote the adsorption of hydroxyl ions (OH). This dual-active-site design effectively reduces the water dissociation energy barrier, thereby accelerating HER process. The electronic interaction between the Pt single atoms and the NiO/Ni heterostructure results in an increased occupation of the Pt 5d orbital, enhancing the catalyst's conductivity and electron transfer capabilities, which further promote the HER process. In 1 M KOH electrolyte, the PtSA-NiO/Ni catalyst exhibits remarkable HER performance, achieving a current density of 10 mA cm^2 at a low overpotential of 26 mV, with a mass activity of 20.6 A mg^{-1} (Pt), significantly surpassing that of commercial Pt/C catalysts. Wang *et al.*[116] successfully synthesized $Mo_2TiC_2T_x$ nanosheets rich in Mo vacancies using an electrochemical exfoliation method, and skillfully anchored Pt single atoms onto the Mo defect sites of the MXene material during HER process through *in situ* synthesis

Table 8 A comparison of catalytic HER performances for the metal boride-based catalysts

Catalyst	Electrolysis test	Electrolyte	Current density (mA cm^{-2})	Overpotential (mV)	Tafel slope (mV dec^{-1})	Ref.
Pd_2B	HER	0.5 M H_2SO_4	10	15.3	22.5	109
α-MoB_2	HER	0.5 M H_2SO_4	100(1000)	149 (334)	74.2	110
P-NCB	HER	1 M KOH	10	37	96	111
	OER	1 M KOH	10	297	48.2	
Ni_xB/f-MWCNT	HER	1 M KOH	10	116	70.4	112
	OER	1 M KOH	10	286	46.3	
Pt/MoB-M	HER	0.5 M H_2SO_4	10	13	24	113

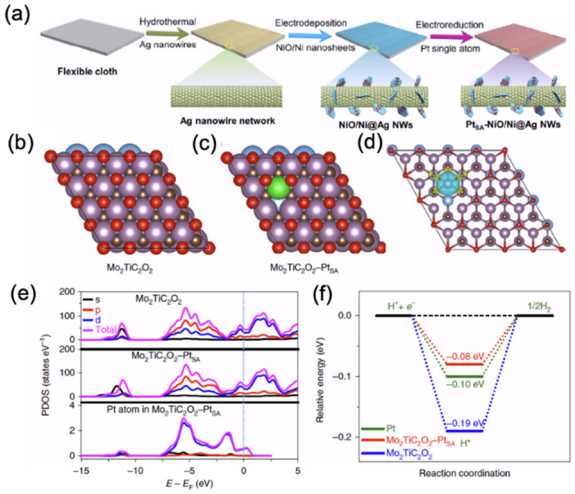

Fig. 17 (a) The synthesis process of PtSA-NiO/Ni catalyst.[115] Top view of the slab models used to describe (b) $Mo_2TiC_2O_2$ and (c) $Mo_2TiC_2O_2$-PtSA. (d) Calculated charge density distribution differences. (e) Calculated PDOS. (f) Calculated free energy profiles of HER at the equilibrium potential.[116]

technology. Specifically, H^+ ions in the acidic solution interacted with the Mo–O bonds in the MXene material. This chemical reaction not only promoted the efficient evolution of hydrogen, but also gradually exfoliated the MXene material into stable nanosheet structures as the hydrogen evolution process continued. Meanwhile, the interaction between H^+ ions and Mo–O bonds also induced the formation of Mo–OH_2 groups, thereby generating more Mo defect sites in the material. These Mo defect sites provided ideal anchoring positions for Pt ions, ultimately resulting in the formation of the $Mo_2TiC_2T_x$-PtSA structure. In 0.5 M H_2SO_4 solution, the $Mo_2TiC_2T_x$-PtSA catalyst exhibited overpotentials of 30, 77, and 104 mV at current densities of 10 mA cm^{-2}, 100 mA cm^{-2}, and 200 mA cm^{-2} respectively. DFT calculations revealed that the electrocatalytic primarily occurred on the Mo–O bonds of the pristine $Mo_2TiC_2T_x$ material surface; however, after the introduction of Pt single atoms, the catalytic active sites shifted to the Pt single atoms, which significantly reduced the activation energy during the electrocatalytic HER process, thereby markedly enhancing its catalytic performance for hydrogen evolution (Fig. 17b–f). Wu *et al.* have successfully employed phosphorus nitride nanotubes as a support to synthesize a ruthenium single-atom catalyst (Ru SAs/PN) with nitrogen coordination. In 0.5 M H_2SO_4 solution, the Ru SAs/PN catalyst demonstrates remarkable performance, requiring a low overpotential of 24 mV at a current density of 10 mA cm^{-2} and exhibiting a high turnover frequency. This performance surpasses that of catalysts where ruthenium single atoms are supported on carbon nitride or porous carbon. Further insights into the differences in catalytic activity of ruthenium single atoms anchored on various supports are provided by DFT calculations. For Ru/C, Ru SAs@C_3N_4, and Ru SAs@C, the Gibbs free energy of ΔG_{H^*} is calculated to be −0.37, −0.32, and −0.44 eV, respectively. These results indicate that the adsorption of H on these surfaces is overly strong, leading to a diminished HER activity. In contrast, the ΔG_{H^*} of Ru SA@PN is −0.27 eV, which is closer to that of the Pt/C catalyst than that of ruthenium single atoms on other supports. Consequently, the hydrogen adsorption–desorption behavior of Ru SAs@PN is favorable for enhancing the overall HER performance.[117]

Shan *et al.*[118] systematically developed a series of single-atom Pt catalysts confined within the lattices of oxides such as Co_3O_4, Mn_5O_8, NiO, and Fe_2O_3, and conducted an in-depth investigation into the relationship between the HER performance of these single-atom catalysts and their respective supports. The study revealed that Pt atoms exhibited diverse geometric topologies in different oxide supports. By judiciously selecting the support, the Pt–Pt interactions could be tuned more flexibly, leading to alterations in the bonding and antibonding orbitals with H. Furthermore, this system was successfully extended to other single-atom systems (*e.g.*, Ru, Pd), demonstrating that catalysts supported on different oxide supports exhibited varying ΔG_{H^*} values. Ultimately, the study established a structure–activity relationship in the form of a "volcano plot", unveiling the intrinsic correlation between single-atom Pt catalysts supported on different oxide carriers and their HER performance. Zhao *et al.*[119] employed a straightforward one-step calcination method to synthesize nickel iodide (Ni-I) precursor. Subsequently, through cyclic voltammetry activation in an alkaline solution, the majority of the iodine atoms in Ni-I were substituted by oxygen atoms and hydroxide ions, yielding a single-atom iodine-based catalyst (SANi-I) supported on nickel hydroxide. *In situ* Raman spectroscopy investigations revealed the formation of I–H intermediates on iodine atoms during HER, indicating that the iodine atoms facilitate the dissociative adsorption of water and hydrogen adsorption. Based on the experimental findings, a plausible reaction pathway for HER on the SANi-I catalyst is proposed. Specifically, water molecules undergo dissociative adsorption at the sites of iodine atoms and adjacent nickel atoms, forming I–H intermediates and OH groups adsorbed on the nickel atoms. Subsequently, two adsorbed hydrogen atoms combine to form molecular hydrogen during the rate-limiting Tafel step.

Table 9 A comparison of catalytic HER performances for the single-atom catalysts

Catalyst	Electrolysis test	Electrolyte	Current density (mA cm^{-2})	Overpotential (mV)	Tafel slope (mV dec^{-1})	Ref.
PtSA-NiO/Ni	HER	1 M KOH	10(100)	26(85)	27.07	115
$Mo_2TiC_2T_x$	HER	0.5 M H_2SO_4	10(100)	30(77)	30	116
Ru SAs@PN	HER	0.5 M H_2SO_4	10	24	38	117

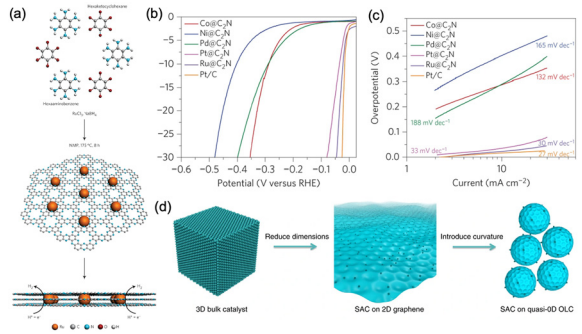

Fig. 18 (a) Schematic illustration of the Ru@C_2N electrocatalyst, (b) LSV curves in 0.5 M H_2SO_4 solution, (c) LSV curves in 1.0 M KOH solution.[121] (d) Schematic diagram of the synthesis of Pt_1/OLC.[123]

The catalytic HER performances of various the single-atom catalysts electrodes are compared in Table 9.

3.10 Carbon-supported catalysts

Carbon materials themselves typically exhibit high inertness and low catalytic activity in the electrocatalytic hydrogen evolution process. However, nanocarbon materials, such as graphene, carbon fibers, and carbon nanotubes, are often used as structural supports to disperse catalysts and simultaneously enhance the electron transport capability of the catalysts, owing to their high electrical conductivity, ease of functionalization, and resistance to acid and alkali corrosion. Therefore, using carbon materials as substrates to load active species has become an effective strategy to improve the activity of HER.[120]

Baek *et al.*[121] reported the synthesis of ruthenium nanoparticles dispersed within a nitrogen-doped porous two-dimensional carbon structure (Ru@C_2N), as depicted in Fig. 18a. The Ru@C_2N electrocatalyst exhibited a high HER turnover frequency (TOF) of 0.67 H_2 s^{-1} in 0.5 M H_2SO_4 solution and 0.75 H_2 s^{-1} in 1.0 M KOH solution at 25 mV, alongside low overpotentials of 13.5 mV in 0.5 M H_2SO_4 and 17.0 mV in 1.0 M KOH at 10 mA cm^{-2}, as shown in Fig. 18b and c, respectively. Furthermore, the Ru@C_2N catalyst demonstrated exceptional stability in both acidic and alkaline media. DFT calculations revealed that the hydrogen binding energy on the surface of Ru_{55}@C_2N was 0.55 eV H^{-1}, which is comparable to that on Pt(111), suggesting an optimal Ru binding energy that facilitates rapid proton adsorption, reduction, and hydrogen evolution processes. Liu *et al.*[122] successfully anchored uniformly dispersed Ir nanoclusters onto N,S-doped graphene through an N,S coordination strategy, synthesizing the Ir-NSG catalyst. Under neutral HER conditions, Ir-NSG exhibited an overpotential of only 22 mV at a current density of 10 mA cm^{-2}, and a high mass activity of 299.52 mA mg^{-1} Ir at an overpotential of 15 mV. Furthermore, electrochemical test results demonstrated that Ir-NSG exhibits excellent intrinsic activity and stability for both HER and OER across the full pH range. The N and S elements firmly anchor the Ir nanoclusters to the graphene surface by forming Ir–N and Ir–S bonds, creating a core–shell structure that enhances the catalyst's stability and catalytic activity. DFT calculations further revealed that the coordination environment of the Ir sites on the Ir-NSG catalyst surface with nitrogen and sulfur optimizes the adsorption energy of reaction intermediates, resulting in a weaker hydrogen chemisorption strength on the catalyst surface. This facilitates the hydrogen desorption step, thereby significantly enhancing HER activity. Song *et al.*[123] deposited isolated Pt atoms (Pt_1/OLC) on zero-dimensional carbon onion-like (OLC) supports *via* atomic layer deposition (ALD) technique (Fig. 18d). In acidic media, the Pt_1/OLC catalyst exhibited a low overpotential of only 38 mV at a current density of 10 mA cm^{-2}, outperforming graphene-supported single-atom catalysts with similar Pt loadings and being comparable to commercial Pt/C catalysts with 20 wt% Pt. Both experimental results and DFT calculations revealed that, benefiting from the high curvature of the OLC support surface, the Pt sites on the Pt_1/OLC catalyst constituted tips and generated localized electric field effects, inducing proton aggregation around the Pt sites and facilitating the proton-coupled electron transfer (PECT) process, ultimately exhibiting superior HER performance.

The catalytic HER performances of various carbon-supported catalysts electrodes are compared in Table 10.

4. Conclusions and prospects

The escalating global energy crisis necessitates an urgent demand for clean and renewable energy sources. Hydrogen production technology, specifically through water electrolysis, is widely recognized as a pivotal technology in the future transformation of the energy structure due to its

Table 10 A comparison of catalytic HER performances for the carbon-supported catalysts

Catalyst	Electrolysis test	Electrolyte	Current density (mA cm^{-2})	Overpotential (mV)	Tafel slope (mV dec^{-1})	Ref.
Ru@C_2N	HER	0.5 M H_2SO_4	10	13.5	30	121
		1 M KOH	10	17	38	
Ir-NSG	HER	1 M PBS	10	22	21.2	122
		0.1 M $HClO_4$	10	17	19.2	
		1 M KOH	10	18.5	28.3	
	OER	1 M PBS	10	307	74.2	
		0.1 M $HClO_4$	10	265	44.2	
		1 M KOH	10	18.5	28.3	
Pt_1/OLC	HER	0.5 M H_2SO_4	10	38	36	123

environmentally friendly and highly efficient renewable characteristics. Enhancing the performance of electrocatalysts, as core components in the hydrogen production process *via* water electrolysis, is crucial for reducing costs and increasing efficiency. After conducting a comprehensive analysis of recent advancements in HER electrocatalysts, we have drawn several conclusions (Fig. 19).

Firstly, there is a discernible trend toward diversification and optimization of catalyst types. Pt-group metal catalysts, due to their excellent catalytic activity and stability, have long dominated the field of electrolysis water hydrogen production catalysts. However, as scientific research has progressed, researchers have gradually discovered that in certain reaction conditions, many non-precious metal catalysts, such as transition metal sulfides, nitrides, carbides, and borides, can also exhibit excellent hydrogen evolution performance. These non-precious metal catalysts not only have lower costs, but also have abundant reserves in the earth's crust, laying a solid foundation for future large-scale applications.

Secondly, catalyst modification strategies are becoming increasingly diverse. To improve the performance of catalysts, researchers have actively explored a variety of modification methods, including increasing the specific surface area of the catalyst, constructing nanostructures, introducing heteroatoms, forming alloys or composite materials, *etc.* These modification strategies not only effectively enhance the catalyst's activity, but also significantly improve its stability and durability, thereby comprehensively enhancing the overall water splitting performance of the catalyst.

Moreover, with the rapid development of characterization techniques and computational chemistry, researchers have gained a deeper understanding of the catalytic mechanism of the catalyst in HER. For example, research has found that the activity of the catalyst is closely related to its electronic structure, surface structure, and the adsorption and desorption process of reaction intermediates. These findings provide important theoretical support for the rational design and optimization of catalysts.

In light of the global energy transition and sustainable development challenges, there remains a pressing need for in-depth research on electrocatalysts for HER. Drawing from our findings, we suggest the following directions for future investigations into electrocatalysts for this reaction:

I. Innovation in non-precious metal catalysts. While platinum group metal catalysts exhibit superior performance, their prohibitive cost and rarity restrict their broad utilization. Consequently, there is a pressing need to intensify research efforts on the development of innovative non-precious metal catalysts, aiming to discover more cost-effective yet high-performing materials.

II. Comprehensive analysis and optimization of catalyst modification strategies. Given the current challenges and limitations associated with catalysts, it is imperative that future research persistently investigates and refines catalyst modification techniques. Through rigorous examination of the structure-performance correlation and reaction mechanisms of catalysts, we can achieve more nuanced control over their performance.

III. Enhancing research on catalytic mechanisms. With the continuous development of characterization techniques and computational chemistry, more emphasis should be placed on the study of catalytic mechanisms in the future. By deeply studying the microscopic structures and dynamic changes of catalysts in the reaction process, the intrinsic and regular catalytic mechanisms can be revealed, providing solid theoretical support for the rational design and optimization of catalysts.

IV. Enhancing interdisciplinary collaboration and exchange. Research on hydrogen evolution electrocatalysts involves multiple disciplines such as chemistry, physics, and materials science. In the future, interdisciplinary cooperation and exchange should be strengthened to jointly promote the development of water electrolysis technology. By pooling wisdom and resources from various parties, we can collectively address the challenges of energy transition and sustainable development.

In summary, research on hydrogen evolution electrocatalysts is currently experiencing a period of rapid development, and there is still great potential and exploration space for the future. Through continuous in-depth research and innovation, we are expected to achieve more efficient and economical electrolysis hydrogen production technology, contributing important forces to the transformation of global energy structure and sustainable development.

Fig. 19 Challenges and prospects of HER electrocatalysts.

Data availability

Data availability is not applicable to this article as no new data were created or analysed in this study.

Author contributions

Conceptualization & supervision: L. Zhou, Z. Zhao, W. Kang and S. B. Aidarova; writing – original draft: J. Shi, Y. Bao, R. Ye and J. Zhong; writing – review and editing: L. Zhou, Z. Zhao, W. Kang and S. B. Aidarova; funding acquisition: L.

Zhou and Z. Zhao. All authors have read and agreed to the published version of the manuscript.

Conflicts of interest

There are no conflicts to declare.

Acknowledgements

This work was supported by National Key R&D Program of China (2022YFB3504100); Liaoning Province international science and technology cooperation program project (2024JH2/102100004); National Natural Science Foundation of China (22102108); Fundamental Research Funds for the Liaoning Universities (LJ212410166075); Youth Foundation of the Education Department of Liaoning Province (LQN202004).

References

1 A. Goyal, S. Louisia, P. Moerland and M. T. M. Koper, Cooperative effect of cations and catalyst structure in tuning alkaline hydrogen evolution on Pt electrodes, *J. Am. Chem. Soc.*, 2024, **146**(11), 7305–7312.
2 Q. Fu, J. Han, X. Wang, P. Xu, T. Yao, J. Zhong, W. Zhong, S. Liu, T. Gao, Z. Zhang, L. Xu and B. Song, 2D Transition metal dichalcogenides: design, modulation, and challenges in electrocatalysis, *Adv. Mater.*, 2020, **33**(6), 1907818–1907841.
3 A. H. Shah, Z. Zhang, C. Wan, S. Wang, A. Zhang, L. Wang, A. N. Alexandrova, Y. Huang and X. Duan, Platinum surface water orientation dictates hydrogen evolution reaction kinetics in alkaline media, *J. Am. Chem. Soc.*, 2024, **146**(14), 9623–9630.
4 Z. Li, S. Xin, Y. Zhang, Z. Zhang, C. Li, C. Li, R. Bao, J. Yi, M. Xu and J. Wang, Boosting elementary steps kinetics towards energetic alkaline hydrogen evolution via dual sites on phase-separated Ni–Cu–Mn/hydroxide, *Chem. Eng. J.*, 2023, 451–459.
5 L. Liu, Y. Liu and C. Liu, Enhancing the Understanding of hydrogen evolution and oxidation reactions on Pt(111) through Ab initio simulation of electrode/electrolyte kinetics, *J. Am. Chem. Soc.*, 2020, **142**(11), 4985–4989.
6 Q. Qin, H. Jang, X. Jiang, L. Wang, X. Wang, M. G. Kim, S. Liu, X. Liu and J. Cho, Constructing interfacial oxygen vacancy and ruthenium lewis acid–base Pairs to Boost the Alkaline Hydrogen Evolution Reaction Kinetics, *Angew. Chem.*, 2024, **136**(3), 202317622–202317623.
7 X. Wang, Z. Wang, Y. Cao, X. Liu, L. Zhou, J. Shi, B. Guo, D. Li, R. Ye and Z. Zhao, A facile synthesis of hierarchical $CoFe_2O_4$ nanosheets for efficient oxygen evolution in neutral medium, *J. Solid State Chem.*, 2024, **331**, 124553–124560.
8 Z. W. Seh, J. Kibsgaard, C. F. Dickens, I. Chorkendorff, J. K. Nørskov and T. F. Jaramillo, Combining theory and experiment in electrocatalysis: Insights into materials design, *Science*, 2017, **355**(6321), 4998–5009.
9 G. Wang, L. Zhang and J. Zhang, A review of electrode materials for electrochemical supercapacitors, *Chem. Soc. Rev.*, 2012, **41**(2), 797–828.
10 V. Etacheri, R. Marom, R. Elazari, G. Salitra and D. Aurbach, Challenges in the development of advanced Li-ion batteries: a review, *Energy Environ. Sci.*, 2011, **4**(9), 3243–3262.
11 J. S. Kim, B. Kim, H. Kim and K. Kang, Recent progress on multimetal oxide catalysts for the oxygen evolution reaction, *Adv. Energy Mater.*, 2018, **8**(11), 1702774–1702781.
12 Z. Lei, T. Wang, B. Zhao, W. Cai, Y. Liu, S. Jiao, Q. Li, R. Cao and M. Liu, Recent progress in electrocatalysts for acidic water oxidation, *Adv. Energy Mater.*, 2020, **10**(23), 2000478–2000495.
13 Y. Wan, L. Zhou and R. Lv, Rational design of efficient electrocatalysts for hydrogen production by water electrolysis at high current density, *Mater. Chem. Front.*, 2023, **7**(23), 6035–6060.
14 A. J. Shih, M. C. O. Monteiro, F. Dattila, D. Pavesi, M. Philips, A. H. M. da Silva, R. E. Vos, K. Ojha, S. Park, O. van der Heijden, G. Marcandalli, A. Goyal, M. Villalba, X. Chen, G. T. K. K. Gunasooriya, I. McCrum, R. Mom, N. López and M. T. M. Koper, Water electrolysis, *Nat. Rev. Methods Primers*, 2022, **2**(1), 84–102.
15 É. Lèbre, M. Stringer, K. Svobodova, J. R. Owen, D. Kemp, C. Côte, A. Arratia-Solar and R. K. Valenta, The social and environmental complexities of extracting energy transition metals, *Nat. Commun.*, 2020, **11**(1), 1–8.
16 Y. Zang, D. Q. Lu, K. Wang, B. Li, P. Peng, Y.-Q. Lan and S. Q. Zang, A pyrolysis-free Ni/Fe bimetallic electrocatalyst for overall water splitting, *Nat. Commun.*, 2023, **14**(1), 1792.
17 Z. Zhang, C. Feng, C. Liu, M. Zuo, L. Qin, X. Yan, Y. Xing, H. Li, R. Si, S. Zhou and J. Zeng, Electrochemical deposition as a universal route for fabricating single-atom catalysts, *Nat. Commun.*, 2020, **11**(1), 1215–1222.
18 W. J. Jiang, T. Tang, Y. Zhang and J. S. Hu, Synergistic modulation of non-precious-metal electrocatalysts for advanced water splitting, *Acc. Chem. Res.*, 2020, **53**(6), 1111–1123.
19 S. Wang, Q. Jiang, S. Ju, C.-S. Hsu, H. M. Chen, D. Zhang and F. Song, Identifying the geometric catalytic active sites of crystalline cobalt oxyhydroxides for oxygen evolution reaction, *Nat. Commun.*, 2022, **13**(1), 6650–6666.
20 J. He, T. Tao, F. Yang and Z. Sun, Unravelling Li^+ intercalation mechanism and cathode electrolyte interphase of $Na_3V_2(PO_4)_3$ and $Na_3(VOPO_4)_2F$ cathode as robust framework towards high-performance lithium-ion batteries, *ChemSusChem*, 2022, **15**(15), 202200817–202200829.
21 X. Wang, S. Xi, P. Huang, Y. Du, H. Zhong, Q. Wang, A. Borgna, Y. W. Zhang, Z. Wang, H. Wang, Z. G. Yu, W. S. V. Lee and J. Xue, Pivotal role of reversible NiO_6 geometric conversion in oxygen evolution, *Nature*, 2022, **611**(7937), 702–708.
22 J. Chen, M. Aliasgar, F. B. Zamudio, T. Zhang, Y. Zhao, X. Lian, L. Wen, H. Yang, W. Sun, S. M. Kozlov, W. Chen and

L. Wang, Diversity of platinum-sites at platinum/fullerene interface accelerates alkaline hydrogen evolution, *Nat. Commun.*, 2023, **14**(1), 1711–1722.

23 B. Gao, Y. Zhao, X. Du, D. Qian, S. Ding, C. Xiao, J. Wang, Z. Song and H. W. Jang, Modulating trinary-heterostructure of MoS_2 via controllably carbon doping for enhanced electrocatalytic hydrogen evolution reaction, *Adv. Funct. Mater.*, 2023, **33**(22), 2214085–2214097.

24 C. Pei, M. C. Kim, Y. Li, C. Xia, J. Kim, W. So, X. Yu, H. S. Park and J. K. Kim, Electron transfer-induced metal spin-crossover at $NiCo_2S_4/ReS_2$ 2D-2D interfaces for promoting pH-universal hydrogen evolution reaction, *Adv. Funct. Mater.*, 2022, **33**(4), 2210072–2210082.

25 Y. Chen, L. Yang, C. Li, Y. Wu, X. Lv, H. Wang and J. E. Qu, In situ Hydrothermal Oxidation of Ternary FeCoNi Alloy Electrode for Overall Water Splitting, *Energy Environ. Mater.*, 2023, **7**(2), 12590–12599.

26 J. Wang, F. Xu, H. Jin, Y. Chen and Y. Wang, Non-noble metal-based carbon composites in hydrogen evolution reaction: fundamentals to applications, *Adv. Mater.*, 2017, **29**(14), 1605838–1605872.

27 T. Wu, Y. Sun, X. Ren, J. Wang, J. Song, Y. Pan, Y. Mu, J. Zhang, Q. Cheng, G. Xian, S. Xi, C. Shen, H. J. Gao, A. C. Fisher, M. P. Sherburne, Y. Du, J. W. Ager, J. Gracia, H. Yang, L. Zeng and Z. J. Xu, Reconstruction of thiospinel to active sites and spin channels for water oxidation, *Adv. Mater.*, 2022, **35**(2), 220704–220716.

28 P. Chen, T. Zhou, M. Zhang, Y. Tong, C. Zhong, N. Zhang, L. Zhang, C. Wu and Y. Xie, 3D Nitrogen-anion-decorated nickel sulfides for highly efficient overall water splitting, *Adv. Mater.*, 2017, **29**(30), 1701584–1701589.

29 Y. Xue, Z. Zuo, Y. Li, H. Liu and Y. Li, Graphdiyne-supported $NiCo_2S_4$ nanowires: A highly active and stable 3D bifunctional electrode material, *Small*, 2017, **13**(31), 1700936–1700945.

30 Z. Li, Y. Zhou, M. Xie, H. Cheng, T. Wang, J. Chen, Y. Lu, Z. Tian, Y. Lai and G. Yu, High-density cationic defects coupling with local alkaline-enriched environment for efficient and stable water oxidation, *Angew. Chem., Int. Ed.*, 2023, **62**(26), 202217815–202217823.

31 Q. Li, H. Zhu, X. Chen, H. Liu, Y. Ren, Y. Chen, K. Ohara, L. Zhou, J. Chen, J. Deng, J. Miao, K. Lin, X. Kuang and X. Xing, Local structure insight into hydrogen evolution reaction with bimetal nanocatalysts, *J. Am. Chem. Soc.*, 2022, **144**(44), 20298–20305.

32 N. Dubouis and A. Grimaud, The hydrogen evolution reaction: from material to interfacial descriptors, *Chem. Sci.*, 2019, **10**(40), 9165–9181.

33 J. Kwon, S. Sun, S. Choi, K. Lee, S. Jo, K. Park, Y. K. Kim, H. B. Park, H. Y. Park, J. H. Jang, H. Han, U. Paik and T. Song, Tailored electronic structure of Ir in high entropy alloy for highly active and durable bifunctional electrocatalyst for water splitting under an acidic environment, *Adv. Mater.*, 2023, **35**(26), 2300091–2300101.

34 W. Liu, Z. Xiao, S. Chandrasekaran, D. Fan, W. Li, H. Lu and Y. Liu, Insights into the effect of sulfur incorporation into tungsten diphosphide for improved hydrogen evolution reaction, *ACS Appl. Mater. Interfaces*, 2022, **14**(14), 16157–16164.

35 L. Zhang, X. Guo, S. Zhang, T. Frauenheim and S. Huang, Hybrid double atom catalysts for hydrogen evolution reaction: a sweet marriage of metal and nonmetal, *Adv. Energy Mater.*, 2023, **14**(2), 2302754–2302763.

36 Q. Yu, X. Liu, G. Liu, X. Wang, Z. Li, B. Li, Z. Wu and L. Wang, Constructing three-phase heterojunction with 1D/3D hierarchical structure as efficient trifunctional electrocatalyst in alkaline seawater, *Adv. Funct. Mater.*, 2022, **32**(46), 2205767–2205776.

37 C. Wang, J. Zhao, X. Du, S. Sun, X. Yu, X. Zhang, Z. Lu, L. Li and X. Yang, Hydrogen production from ammonia borane hydrolysis catalyzed by non-noble metal-based materials: a review, *J. Mater. Sci.*, 2020, **56**(4), 2856–2878.

38 X. Zeng, Y. Zhao, X. Hu, G. D. Stucky and M. Moskovits, Rational component and structure design of noble-metal composites for optical and catalytic applications, *Small Struct.*, 2021, **2**(4), 2000138–2000162.

39 X. Zou and Y. Zhang, Noble metal-free hydrogen evolution catalysts for water splitting, *Chem. Soc. Rev.*, 2015, **44**(15), 5148–5180.

40 M. Jahan, Z. Liu and K. P. Loh, A graphene oxide and copper-centered metal organic framework composite as a tri-functional catalyst for HER, OER, and ORR, *Adv. Funct. Mater.*, 2013, **23**(43), 5363–5372.

41 S. Gao, Y. Zhang, Y. Zhang, B. Wang and S. Yang, Modification of carbon nanotubes via birch reaction for enhanced HER catalyst by constructing pearl necklace-like $NiCo_2P_2$-CNT composite, *Small*, 2018, **14**(51), 1804388–1804400.

42 Q. Li, Q. Zhang, W. Xu, R. Zhao, M. Jiang, Y. Gao, W. Zhong, K. Chen, Y. Chen, X. Li and N. Yang, Sowing single atom seeds: a versatile strategy for hyper-low noble metal loading to boost hydrogen evolution reaction, *Adv. Energy Mater.*, 2023, **13**(10), 2203955–2203964.

43 M. Kim, S. H. Kim, J. Park, S. Lee, I. Jang, S. Kim, C. Y. Lee, O. J. Kwon, H. C. Ham, J. T. Hupp, N. Jung, S. J. Yoo and D. Whang, Reconstructing Oxygen-deficient zirconia with ruthenium catalyst on atomic-scale interfaces toward hydrogen production, *Adv. Funct. Mater.*, 2023, **33**(29), 2300673–2300681.

44 R. Zhang, Y. Li, X. Zhou, A. Yu, Q. Huang, T. Xu, L. Zhu, P. Peng, S. Song, L. Echegoyen and F. F. Li, Single-atomic platinum on fullerene C60 surfaces for accelerated alkaline hydrogen evolution, *Nat. Commun.*, 2023, **14**(1), 2460–2471.

45 Y. Zhu, K. Fan, C. S. Hsu, G. Chen, C. Chen, T. Liu, Z. Lin, S. She, L. Li, H. Zhou, Y. Zhu, H. M. Chen and H. Huang, Supported ruthenium single-atom and clustered catalysts outperform benchmark Pt for alkaline hydrogen evolution, *Adv. Mater.*, 2023, **35**(35), 2301133–2301140.

46 Z. Yu, X. Rui and Y. Yu, Hydrogen spillover in Pt_5Ru nanoalloy decorated Ni_3S_2 enabling pH-universal electrocatalytic hydrogen evolution, *EES Catal.*, 2023, **1**(5), 695–703.

47 H. Shi, X. Y. Sun, S. P. Zeng, Y. Liu, G. F. Han, T. H. Wang, Z. Wen, Q. R. Fang, X. Y. Lang and Q. Jiang, Nanoporous nonprecious high-entropy alloys as multisite electrocatalysts for ampere-level current-density hydrogen cevolution, *Small Struct.*, 2023, **4**(9), 2300042–2300049.

48 F. Lyu, S. Zeng, Z. Jia, F.-X. Ma, L. Sun, L. Cheng, J. Pan, Y. Bao, Z. Mao, Y. Bu, Y. Y. Li and J. Lu, Two-dimensional mineral hydrogel-derived single atoms-anchored heterostructures for ultrastable hydrogen evolution, *Nat. Commun.*, 2022, **13**(1), 6249–6260.

49 J. Zhang, J. Wu, X. Zou, K. Hackenberg, W. Zhou, W. Chen, J. Yuan, K. Keyshar, G. Gupta, A. Mohite, P. M. Ajayan and J. Lou, Discovering superior basal plane active two-dimensional catalysts for hydrogen evolution, *Mater. Today*, 2019, **25**, 28–34.

50 M. Zhou, X. Jiang, W. Kong, H. Li, F. Lu, X. Zhou and Y. Zhang, Synergistic effect of dual-doped carbon on Mo_2C nanocrystals facilitates alkaline hydrogen evolution, *Nano-Micro Lett.*, 2023, **15**(1), 166–176.

51 Z. Chen, W. Gong, J. Wang, S. Hou, G. Yang, C. Zhu, X. Fan, Y. Li, R. Gao and Y. Cui, Metallic W/WO_2 solid-acid catalyst boosts hydrogen evolution reaction in alkaline electrolyte, *Nat. Commun.*, 2023, **14**(1), 5363–5374.

52 J. Wang, T. Liao, Z. Wei, J. Sun, J. Guo and Z. Sun, Heteroatom-doping of non-noble metal-based catalysts for electrocatalytic hydrogen evolution: an electronic structure tuning strategy, *Small Methods*, 2021, **5**(4), 2000988–2001014.

53 Z. Huang, T. Cheng, A. H. Shah, G. Zhong, C. Wan, P. Wang and X. Duan, Edge sites dominate the hydrogen evolution reaction on platinum nanocatalysts, *Nat. Catal.*, 2024, 1–11.

54 H. Zhang, K. Chi, L. Qiao, P. Gao, Z. Li, X. Guo and D. Cheng, Boosting acidic hydrogen evolution kinetics induced by weak strain effect in PdPt alloy for proton exchange membrane water electrolyzers, *Small*, 2024, **20**(51), 2406935–2406944.

55 S. Qiao, Q. He, Q. Zhou, Y. Zhou, W. Xu, H. Shou, Y. Cao, S. Chen, X. Wu and L. Song, Interfacial electronic interaction enabling exposed Pt(110) facets with high specific activity in hydrogen evolution reaction, *Nano Res.*, 2022, **16**(1), 174–180.

56 Y. Jia, T. H. Huang, S. Lin, L. Guo, Y. M. Yu, J. H. Wang, K. W. Wang and S. Dai, Stable Pd-Cu hydride catalyst for efficient hydrogen evolution, *Nano Lett.*, 2022, **22**(3), 1391–1397.

57 Z. Zhai, Y. Wang, C. Si, P. Liu, W. Yang, G. Cheng and Z. Zhang, Self-templating synthesis and structural regulation of nanoporous rhodium-nickel alloy nanowires efficiently catalyzing hydrogen evolution reaction in both acidic and alkaline electrolytes, *Nano Res.*, 2023, **16**(2), 2026–2034.

58 X. Wang, Y. Cao, L. Zhou, Z. Yu, R. Ye, D. Li, B. Guo, X. Liu, L. Zhou and Z. Zhao, Spherical Ru/FeO_x composite as a bifunctional electrocatalyst for overall water splitting in neutral media, *J. Alloys Compd.*, 2024, 177417–177424.

59 Y. Wang, Z. Chen, Q. Li, X. Wang, W. Xiao, Y. Fu, G. Xu, B. Li, Z. Li, Z. Wu and L. Wang, Porous needle-like Fe-Ni-P doped with Ru as efficient electrocatalyst for hydrogen generation powered by sustainable energies, *Nano Res.*, 2022, **16**(2), 2428–2435.

60 S. Xie, C. Huang, H. Dong, B. Xu, Y. Miao, B. Gao and X. Peng, A $MoNi_4$(312) surface preferred reconstruction enhancing hydrogen evolution, *Appl. Catal., B*, 2025, **363**, 124831–124838.

61 H. Kim, E. Hwang, H. Park, B. S. Lee, J. H. Jang, H. J. Kim and S. K. Kim, Non-precious metal electrocatalysts for hydrogen production in proton exchange membrane water electrolyzer, *Appl. Catal., B*, 2017, **206**, 608–616.

62 K. Zhu, J. Chen, W. Wang, J. Liao, J. Dong, M. O. L. Chee, N. Wang, P. Dong, P. M. Ajayan, S. Gao, J. Shen and M. Ye, Etching-doping sedimentation equilibrium strategy: accelerating kinetics on hollow Rh-doped CoFe-layered double hydroxides for water splitting, *Adv. Funct. Mater.*, 2020, **30**(35), 2003556–2003565.

63 Z. Wu, X. Wang, J. Huang and F. Gao, A Co-doped Ni–Fe mixed oxide mesoporous nanosheet array with low overpotential and high stability towards overall water splitting, *J. Mater. Chem. A*, 2018, **6**(1), 167–178.

64 F. F. Dai, Y. X. Xue, D. L. Gao, Y. X. Liu, J. H. Chen, Q. J. Lin, W. W. Lin and Q. Yang, Facile fabrication of self-supporting porous $CuMoO_4$@Co_3O_4nanosheets as a bifunctional electrocatalyst for efficient overall water splitting, *Dalton Trans.*, 2022, **51**(33), 12736–12745.

65 R. Rajalakshmi, G. Srividhya, C. Viswanathan and N. Ponpandian, Hydrogen spillover effect-harnessing hydrogen evolution reaction from diverse carbon-based supports with a tungsten oxide catalyst, *J. Mater. Chem. A*, 2023, **11**(29), 15889–15905.

66 Y. Sun, Y. Bao, D. Yin, X. Bu, Y. Zhang, K. Yue, X. Qi, Z. Cai, Y. Li, X. Hu, J. C. Ho and X. Wang, Oxygen vacancy-induced efficient hydrogen spillover in Ni17W3/WO3−x/MoO3−x for a superior pH-universal hydrogen evolution reaction, *J. Mater. Chem. A*, 2024, **12**(19), 11563–11570.

67 A. I. Inamdar, A. S. Salunke, J. H. Seok, H. S. Chavan, N. K. Shrestha, S. U. Lee, S. Cho and H. Im, Cobalt oxide/cerium oxide heterogeneous interfaces as advanced durable and bifunctional electrocatalysts for robust industrially relevant overall water splitting, *J. Mater. Chem. A*, 2024, **12**(45), 31362–31374.

68 Z. Li, Y. Feng, Y. L. Liang, C. Q. Cheng, C. K. Dong, H. Liu and X. W. Du, Stable Rhodium (IV) oxide for alkaline hydrogen evolution reaction, *Adv. Mater.*, 2020, **32**(25), 1908521–1908527.

69 T. X. Huang, X. Cong, S. S. Wu, J. B. Wu, Y. F. Bao, M. F. Cao and B. Ren, Visualizing the structural evolution of individual active sites in MoS_2 during electrocatalytic hydrogen evolution reaction, *Nat. Catal.*, 2024, 1–9.

70 J. X. Feng, J. Q. Wu, Y. X. Tong and G. R. Li, Efficient hydrogen evolution on Cu nanodots-decorated Ni_3S_2 nanotubes by optimizing atomic hydrogen adsorption and desorption, *J. Am. Chem. Soc.*, 2018, **140**(2), 610–617.

71 T. Ali, W. Qiao, D. Zhang, W. Liu, S. Sajjad, C. Yan and R. Su, Surface sulfur vacancy engineering of metal sulfides

promoted desorption of hydrogen atoms for enhanced electrocatalytic hydrogen evolution, *J. Phys. Chem. C*, 2021, **125**(23), 12707–12712.

72 B. Dong, J. Y. Xie, N. Wang, W. K. Gao, Y. Ma, T. S. Chen, X. T. Yan, Q. Z. Li, Y. L. Zhou and Y. M. Chai, Zinc ion induced three-dimensional Co_9S_8 nano-neuron network for efficient hydrogen evolution, *Renewable Energy*, 2020, **157**, 415–423.

73 H. J. Liu, S. Zhang, Y. M. Chai and B. Dong, Ligand modulation of active sites to promote Cobalt-doped-1T-MoS_2 electrocatalytic hydrogen evolution in alkaline media, *Angew. Chem., Int. Ed.*, 2023, **62**(48), 202313845–202313855.

74 Y. Takahashi, Y. Kobayashi, Z. Wang, Y. Ito, M. Ota, H. Ida, A. Kumatani, K. Miyazawa, T. Fujita, H. Shiku, Y. E. Korchev, Y. Miyata, T. Fukuma, M. Chen and T. Matsue, High-resolution electrochemical mapping of the hydrogen evolution reaction on transition-metal dichalcogenide nanosheets, *Angew. Chem., Int. Ed.*, 2020, **59**(9), 3601–3608.

75 W. Zhan, X. Zhai, Y. Li, M. Wang, H. Wang, L. Wu, X. Tang, H. Zhang, B. Ye, K. Tang, G. Wang and M. Zhou, Regulating local atomic environment around cvacancies for efficient hydrogen evolution, *ACS Nano*, 2024, **18**(14), 10312–10323.

76 Y. Park, H. K. Kim, T. Kwon, M. Jun, D. Kim, T. Kim and K. Lee, Boosting hydrogen evolution reaction on Co_9S_8 in neutral media leveraging oxophilic CrO_x mosaic dopant, *Adv. Energy Mater.*, 2024, 2405035–2405044.

77 X. Bai, M. Zhang, Y. Shen, X. Liang, W. Jiao, R. He and X. Zou, Room-temperature, meter-scale synthesis of heazlewoodite-based nanoarray electrodes for alkaline water electrolysis, *Adv. Funct. Mater.*, 2024, 2400979–2400987.

78 A. Morozan, H. Johnson, C. Roiron, G. Genay, D. Aldakov, A. Ghedjatti and V. Artero, Nonprecious bimetallic iron–molybdenum sulfide electrocatalysts for the hydrogen evolution reaction in proton exchange membrane electrolyzers, *ACS Catal.*, 2020, **10**(24), 14336–14348.

79 L. Zhou, Z. Han, W. Li, W. Leng, Z. Yu and Z. Zhao, Hierarchical Co–Mo–S nanoflowers as efficient electrocatalyst for hydrogen evolution reaction in neutral media, *J. Alloys Compd.*, 2020, **844**, 156108–156116.

80 Y. Hou, M. R. Lohe, J. Zhang, S. Liu, X. Zhuang and X. Feng, Vertically oriented cobalt selenide/NiFe layered-double-hydroxide nanosheets supported on exfoliated graphene foil: an efficient 3D electrode for overall water splitting, *Energy Environ. Sci.*, 2016, **9**(2), 478–483.

81 R. Li, L. Chen, H. Zhang, M. Humayun, J. Duan, X. Xu, Y. Fu, M. Bououdina and C. Wang, Exceptional green hydrogen production performance of a ruthenium-modulated nickel selenide, *Nanoscale*, 2023, **15**(48), 19604–19616.

82 F. Ming, H. Liang, H. Shi, X. Xu, G. Mei and Z. Wang, MOF-derived Co-doped nickel selenide/C electrocatalysts supported on Ni foam for overall water splitting, *J. Mater. Chem. A*, 2016, **4**(39), 15148–15155.

83 Z. Chen, X. Li, J. Zhao, S. Zhang, J. Wang, H. Zhang, J. Zhang, Q. Dong, W. Zhang, W. Hu and X. Han, Stabilizing Pt single atoms through Pt-Se electron bridges on vacancy-enriched nickel selenide for efficient electrocatalytic hydrogen evolution, *Angew. Chem., Int. Ed.*, 2023, **62**(39), 202308686–202308694.

84 B. Hao, M. Gan, J. Guo, G. Li, Y. Song, Y. Shen and J. Guo, Constructing 2D $PtSe_2$/PtCo heterojunctions by partial selenization for enhanced hydrogen evolution, *Adv. Funct. Mater.*, 2024, 2413916–2413923.

85 J. Chen, B. Ren, H. Cui and C. Wang, Constructing Pure Phase Tungsten-Based Bimetallic Carbide Nanosheet as an Efficient Bifunctional Electrocatalyst for Overall Water Splitting, *Small*, 2020, **16**(23), 1907556–1907563.

86 C. Huang, X. Miao, C. Pi, B. Gao, X. Zhang, P. Qin, K. Huo, X. Peng and P. K. Chu, Mo_2C/VC heterojunction embedded in graphitic carbon network: An advanced electrocatalyst for hydrogen evolution, *Nano Energy*, 2019, **60**, 520–526.

87 Y. Ma, M. Chen, H. Geng, H. Dong, P. Wu, X. Li, G. Guan and T. Wang, Synergistically tuning tlectronic structure of porous β-Mo_2C spheres by Co doping and Mo-vacancies defect engineering for optimizing hydrogen evolution reaction activity, *Adv. Funct. Mater.*, 2020, **30**(19), 2000561–2000574.

88 A. Kagkoura, H. J. Ojeda-Galván, M. Quintana and N. Tagmatarchis, Carbon dots strongly immobilized onto carbon nanohorns as non-metal heterostructure with high electrocatalytic activity towards protons reduction in hydrogen evolution reaction, *Small*, 2023, **19**(31), 2208285–2208291.

89 Y. Zhang, S. Yun, J. Dang, C. Dang, G. Yang, Y. Wang, Z. Liu and Y. Deng, Defect engineering via ternary nonmetal doping boosts the catalytic activity of ZIF-derived carbon-based metal-free catalysts for photovoltaics and water splitting, *Mater. Today Phys.*, 2022, **27**, 100785–100798.

90 W. Liu, Z. Zhang, M. G. Sendeku, J. Yu, T. Li, Z. Wang and X. Sun, Synergistic N-doping and heterointerface engineering in W_2C/W nanoarrays enable pH-universal hydrogen evolution catalysis, *ACS Appl. Eng. Mater.*, 2023, **1**(2), 861–867.

91 Y. Li, Z. Dou, Y. Pan, H. Zhao, L. Yao, Q. Wang and H. Yang, Crystalline phase engineering to modulate the interfacial interaction of the ruthenium/molybdenum carbide for acidic hydrogen evolution, *Nano Lett.*, 2024, **24**(19), 5705–5713.

92 Y. Li, X. Wan, Z. Chen, D. Ding, H. Li, N. Zhang and Y. Cui, Activity enhancement of molybdenum carbide in alkaline hydrogen evolution reaction through oxidation-gradient modulation, *ACS Catal.*, 2024, **14**(22), 16712–16722.

93 Y. Zheng, Y. Mou, Y. Wang, J. Wan, G. Yao, C. Feng and Y. Wang, Aluminum-incorporation activates vanadium carbide with electron-rich carbon sites for efficient pH-universal hydrogen evolution reaction, *J. Colloid Interface Sci.*, 2024, **656**, 367–375.

94 Y. Hong, S. Jeong, J. H. Seol, T. Kim, S. C. Cho, T. K. Lee and K. Lee, Ru_2P/Ir_2P heterostructure promotes hydrogen spillover for efficient alkaline hydrogen evolution reaction, *Adv. Energy Mater.*, 2024, **14**(29), 2401426–2401439.

95 B. Liu, B. Zhong, F. Li, J. Liu, L. Zhao, P. Zhang and L. Gao, Co_2P/CoP heterostructures with significantly enhanced performance in electrocatalytic hydrogen evolution reaction: Synthesis and electron redistribution mechanism, *Nano Res.*, 2023, **16**(11), 12830–12839.

96 M. Liu, Z. Sun, S. Li, X. Nie, Y. Liu, E. Wang and Z. Zhao, Hierarchical superhydrophilic/superaerophobic CoMnP/Ni_2P nanosheet-based microplate arrays for enhanced overall water splitting, *J. Mater. Chem. A*, 2021, **9**(38), 22129–22139.

97 X. D. Wang, Y. F. Xu, H. S. Rao, W. J. Xu, H. Y. Chen, W. X. Zhang, D. B. Kuang and C. Y. Su, Novel porous molybdenum tungsten phosphide hybrid nanosheets on carbon cloth for efficient hydrogen evolution, *Energy Environ. Sci.*, 2016, **9**(4), 1468–1475.

98 W. Liu, P. Geng, S. Li, W. Liu, D. Fan, H. Lu, Z. Lu and Y. Liu, Tuning electronic configuration of WP_2 nanosheet arrays via nickel doping for high-efficiency hydrogen evolution reaction, *J. Energy Chem.*, 2021, **55**, 17–24.

99 D. Chen, Z. Pu, R. Lu, P. Ji, P. Wang, J. Zhu, C. Lin, H. W. Li, X. Zhou, Z. Hu, F. Xia, J. Wu and S. Mu, Ultralow Ru loading transition metal phosphides as high-efficient bifunctional electrocatalyst for a solar-to-hydrogen generation system, *Adv. Energy Mater.*, 2020, **10**(28), 2000814–2000823.

100 X. Ji, X. Chen, L. Zhang, C. Meng, Y. He, X. Zhang, Z. Wang and R. Yu, Anchoring nitrogen-doped Co_2P nanoflakes on $NiCo_2O_4$ nanorod arrays over nickel foam as high-performance 3D electrode for alkaline hydrogen evolution, *Green Energy Environ.*, 2023, **8**(2), 470–477.

101 W. Chen, M. Li, Y. Yu, H. Huo, H. Hou, W. Feng and D. Min, Lattice tensile strain regulated by ruthenium doping in NiCoP anchoring on carbonized wood for promoting hydrogen evolution reaction, *Fuel*, 2025, **383**, 133941–133949.

102 M. Jiang, Y. Li, Z. Lu, X. Sun and X. Duan, Binary nickel–iron nitride nanoarrays as bifunctional electrocatalysts for overall water splitting, *Inorg. Chem. Front.*, 2016, **3**(5), 630–634.

103 L. Yu, Q. Zhu, S. Song, B. McElhenny, D. Wang, C. Wu, Z. Qin, J. Bao, Y. Yu, S. Chen and Z. Ren, Non-noble metal-nitride based electrocatalysts for high-performance alkaline seawater electrolysis, *Nat. Commun.*, 2019, **10**(1), 5106–5115.

104 W. Ma, D. Li, L. Liao, H. Zhou, F. Zhang, X. Zhou and F. Yu, High-performance bifunctional porous iron-rich phosphide/nickel nitride hceterostructures for calkaline cseawater splitting, *Small*, 2023, **19**(19), 2207082–2207091.

105 G. Li, J. Yu, W. Yu, L. Yang, X. Zhang, X. Liu, H. Liu and W. Zhou, Phosphorus-doped iron nitride nanoparticles encapsulated by nitrogen-doped carbon nanosheets on iron foam in situ derived from saccharomycetes cerevisiae for electrocatalytic overall water splitting, *Small*, 2020, **16**(32), 2001980–2001990.

106 J. Tang, S. Zhang, Y. Zeng, B. Yang, K. Zhang, Y. Li, Y. Yao and J. Hu, Porous rod-like structured ternary nitride heterocatalyst Co_3Mo_3N/Ni_3Mo_3N for efficient and stable hydrogen evolution reaction, *Chem. Eng. J.*, 2024, 487–495.

107 L. Zong, F. Lu, P. Li, K. Fan, T. Zhan, P. Liu, L. Jiang, D. Chen, R. Zhang and L. Wang, Thermal shock synthesis for loading Sub-2 nm Ru nanoclusters on titanium nitride as a remarkable electrocatalyst toward hydrogen evolution reaction, *Adv. Mater.*, 2024, **36**, 2403525–2403533.

108 J. Zhao, R. Urrego-Ortiz, N. Liao, F. Calle-Vallejo and J. Luo, Rationally designed Ru catalysts supported on TiN for highly efficient and stable hydrogen evolution in alkaline conditions, *Nat. Commun.*, 2024, **15**(1), 6391–6404.

109 L. Chen, L. R. Zhang, L. Y. Yao, Y. H. Fang, L. He, G. F. Wei and Z. P. Liu, Metal boride better than Pt: HCP Pd_2B as a superactive hydrogen evolution reaction catalyst, *Energy Environ. Sci.*, 2019, **12**(10), 3099–3105.

110 Y. Chen, G. Yu, W. Chen, Y. Liu, G. D. Li, P. Zhu, Q. Tao, Q. Li, J. Liu, X. Shen, H. Li, X. Huang, D. Wang, T. Asefa and X. Zou, Highly active, nonprecious electrocatalyst comprising borophene subunits for the hydrogen evolution reaction, *J. Am. Chem. Soc.*, 2017, **139**(36), 12370–12373.

111 A. T. Sivagurunathan, S. Seenivasan, T. Kavinkumar and D. H. Kim, Phosphorus doping of nickel–cobalt boride to produce a metal–metalloid–nonmetal electrocatalyst for improved overall water splitting, *J. Mater. Chem. A*, 2024, **12**(8), 4643–4655.

112 X. Chen, Z. Yu, L. Wei, Z. Zhou, S. Zhai, J. Chen, Y. Wang, Q. Huang, H. E. Karahan, X. Liao and Y. Chen, Ultrathin nickel boride nanosheets anchored on functionalized carbon nanotubes as bifunctional electrocatalysts for overall water splitting, *J. Mater. Chem. A*, 2019, **7**(2), 764–774.

113 C. Wang, H. Li, W. Xiao, Z. Xiao, G. Xu, D. Chen and L. Wang, Low loading of Pt on MoB constructed by microwave quasi-solid approach with solvent regulation for hydrogen evolution reaction, *J. Colloid Interface Sci.*, 2025, **678**, 1223–1229.

114 H. Cao, Q. Wang, Z. Zhang, H. M. Yan, H. Zhao, H. B. Yang, B. Liu, J. Li and Y. G. Wang, Engineering single-atom electrocatalysts for enhancing kinetics of acidic Volmer reaction, *J. Am. Chem. Soc.*, 2023, **145**(24), 13038–13047.

115 K. L. Zhou, Z. Wang, C. B. Han, X. Ke, C. Wang, Y. Jin and H. Yan, Platinum single-atom catalyst coupled with transition metal/metal oxide heterostructure for accelerating alkaline hydrogen evolution reaction, *Nat. Commun.*, 2021, **12**(1), 3783–3792.

116 J. Zhang, Y. Zhao, X. Guo, C. Chen, C. L. Dong, R. S. Liu and G. Wang, Single platinum atoms immobilized on an MXene as an efficient catalyst for the hydrogen evolution reaction, *Nat. Catal.*, 2018, **1**(12), 985–992.

117 J. Yang, B. Chen, X. Liu, W. Liu, Z. Li, J. Dong and Y. Li, Phosphorus nitride imide nanotube as carbon-free support to anchor single Ru sites for efficient and robust hydrogen evolution, *Angew. Chem., Int. Ed.*, 2018, **57**, 9495–9500.

118 J. Shan, C. Ye, C. Zhu, J. Dong, W. Xu, L. Chen and S. Z. Qiao, Integrating interactive noble metal single-atom catalysts into transition metal oxide lattices, *J. Am. Chem. Soc.*, 2022, **144**(50), 23214–23222.

119 Y. Zhao, T. Ling, S. Chen, B. Jin, A. Vasileff, Y. Jiao and S. Z. Qiao, Non-metal single-iodine-atom electrocatalysts for the hydrogen evolution reaction, *Angew. Chem., Int. Ed.*, 2019, **58**(35), 12252–12257.
120 Y. Liu, Q. Wang, J. Zhang, J. Ding, Y. Cheng, T. Wang and B. Liu, Recent advances in carbon-supported noble-metal electrocatalysts for hydrogen evolution reaction: syntheses, structures, and properties, *Adv. Energy Mater.*, 2022, **12**(28), 2200928.
121 J. Mahmood, F. Li, S. M. Jung, M. S. Okyay, I. Ahmad, S. J. Kim and J. B. Baek, An efficient and pH-universal ruthenium-based catalyst for the hydrogen evolution reaction, *Nat. Nanotechnol.*, 2017, **12**(5), 441–446.
122 Q. Wang, C. Q. Xu, W. Liu, S. F. Hung, H. Bin Yang, J. Gao and B. Liu, Coordination engineering of iridium nanocluster bifunctional electrocatalyst for highly efficient and pH-universal overall water splitting, *Nat. Commun.*, 2020, **11**(1), 4246–4255.
123 D. Liu, X. Li, S. Chen, H. Yan, C. Wang, C. Wu and L. Song, Atomically dispersed platinum supported on curved carbon supports for efficient electrocatalytic hydrogen evolution, *Nat. Energy*, 2019, **4**(6), 512–518.